

with statistically independent nonredundant coefficients due to the linearity of the DFT.

<sup>25</sup>P. D. Welch, "The use of Fast Fourier Transform for the estimation of power spectra: A method based on time averaging over short, modified periodograms," *IEEE Trans. Audio and Electroacoust.*

15, 70-73 (1967).

<sup>26</sup>G. Senge, *Quantization of Image Transforms with Minimum Distortion*, Technical Report No. ECE-77-8, Dept. of Electrical and Computer Engineering, University of Wisconsin-Madison, Madison, Wis., May, 1977 (unpublished).

## Refractoriness in the maintained discharge of the cat's retinal ganglion cell\*

Malvin Carl Teich, Leonard Matin, and Barry I. Cantor

*Columbia University, New York, New York 10027*

(Received 20 September 1976; revision received 16 September 1977)

When effects due to refractoriness (reduction of sensitivity following a nerve impulse) are taken into account, the Poisson process provides the basis for a model which accounts for all of the first-order statistical properties of the maintained discharge in the retinal ganglion cell of the cat. The theoretical pulse-number distribution (PND) and pulse-interval distribution (PID) provide good fits to the experimental data reported by Barlow and Levick for on-center, off-center, and luminance units. The model correctly predicts changes in the shape of the empirical PND with adapting luminance and duration of the interval in which impulses are counted (counting interval). It also requires that a decrease in sensitivity to stimulation by light with increasing adapting luminance occur prior to the ganglion cell and is thus consistent with other data. Under the assumptions of the model, both on-center and off-center units appear to exhibit increasing refractoriness as the adapting luminance increases. Relationships are presented between the PND and PID for Poisson counting processes without refractoriness, with a fixed refractory period, and with a stochastically varying refractory period. It is assumed that events unable to produce impulses during the refractory period do not prolong the duration of the period (nonparalyzable counting). A short refractory period (e.g., 2% of the counting interval) drastically alters both the PND and PID, producing marked decreases in the mean and variance of the PND along with an increase in the ratio of mean to variance. In all cases of interest, a small amount of variability in refractory-period duration distinctly alters the PID from that obtainable with a fixed refractory period but has virtually no effect on the fixed-refractory period PND. Other two-parameter models that invoke scaling of a Poisson input and paralyzable counting yield predictions that do not match the data.

### I. INTRODUCTION

The sequence of impulses recorded from the retinal ganglion cell of the cat remains irregular even when the retina is thoroughly adapted to a steady stimulus of fixed luminance. Though this maintained discharge has been observed in a variety of vertebrates, its main characteristics have been described in greatest detail in the cat.<sup>1-10</sup> Barlow and Levick<sup>6</sup> and Sakmann and Creutzfeldt<sup>7</sup> have noted that the average maintained firing rate of on-center units increases as the adapting luminance is increased from zero up to a point at which the increase is either slowed or reversed with further increases in luminance. At still higher adaptation levels, the firing rate again rises.<sup>3,6</sup> Both Sakmann and Creutzfeldt<sup>7</sup> and Barlow and Levick<sup>6</sup> attribute the plateau or fall in firing rate to increasing contribution from the inhibitory surround. The average firing rate of off-center units tends to decrease with increasing adapting luminance, though the change is neither as consistent nor as large as that observed for on-center units.

The most striking properties of the maintained discharge are the large and increasing compression between numbers of quanta absorbed and nerve impulses generated, and the substantial increase in mean-to-variance ratio of the empirical pulse-number distribution (PND) with increasing luminance.<sup>5</sup> The pulse-number distribution is also often referred to as the

pulse-counting distribution (see Fig. 1). These properties have led workers to consider that scaling and refractoriness mediate between absorbed quanta and the maintained discharge.<sup>1,4-6,8-13</sup> While we employ the term "refractoriness" in its usual sense—to imply a reduction in sensitivity for some period following the occurrence of a neuronal spike—it is important to note that we do not imply that the refractory period we deal with be identified with those normally found in axons following electrical stimulation (see Sec. V for further related considerations). We shall also often employ the term "dead time" to refer to the period following an impulse (spike) during which another impulse cannot occur; this term has its roots in the nuclear physics literature.<sup>14</sup> The terms refractory period and dead time will thus be nearly interchangeable. We use the term "scaling" to refer to a particular kind of reduction in sensitivity in which a system requires  $r$  input events in order to produce a single output event;  $r$  is then the scaling parameter. Barlow and Levick<sup>6</sup> considered such a simple scaling model for the case in which the input events represented Poisson-distributed quanta of light and the output was the discharge of ganglion cell spikes, but found that the required parameter values were seriously wrong. Barlow<sup>12</sup> subsequently criticized this scaling model on other grounds as well, though Levick<sup>9</sup> has recently pointed out that some modifications introduced by Stein<sup>15,16</sup> may improve matters. We develop the simple scaling model further and arrive at a conclusion similar to that arrived at by Barlow.<sup>12</sup>

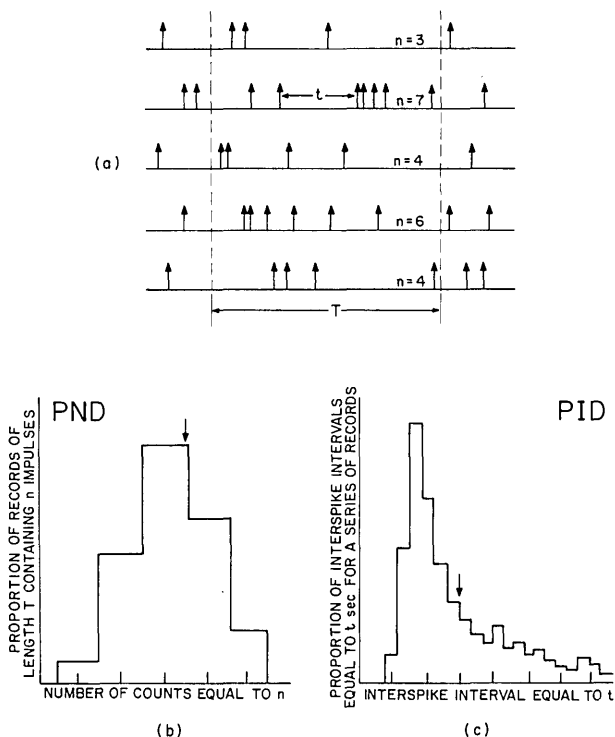


FIG. 1. (a) Five sample records of nerve impulses for a given unit during steady stimulation by light are schematized.  $T$  is the time interval during which a count of nerve impulses ( $n$ ) is taken in each record;  $n$  is equal to 3, 7, 4, 6, and 4 impulses (or counts) in the five records. A single time interval between a pair of impulses in the second record is labeled as  $t$  (interspike interval). (b) Experimental pulse-counting or pulse-number distribution (PND): A relative frequency distribution of  $n$  over a set of sample records such as those in (a). The ordinate represents the proportion of the total number of records in which the value of  $n$  shown on the abscissa was obtained. Arrow indicates mean number of counts. (c) Experimental pulse-interval distribution (PID): A relative frequency distribution of interspike intervals ( $t$ ) over a set of sample records such as in (a). Arrow indicates mean interspike time interval. [The PND shown in (b) and the PID shown in (c) are not drawn from the records in (a)].

Barlow and Levick<sup>6</sup> modeled the recorded discharge by fitting Gaussian distributions to the empirical PND's (mean and variance determined by the experimental data) and gamma distributions to the empirical pulse-interval distributions (PID's); see Fig. 1. (The gamma distribution is the PID of the scaling model with Poisson input.) As Barlow and Levick<sup>6</sup> note, this model works reasonably well empirically although the combination of a Gaussian PND and a gamma PID does not provide a consistent model of the underlying process. Indeed, the PND and PID are intimately linked (see Sec. III).<sup>17</sup> Further, the increasing mean-to-variance ratio of the PND with increasing luminance is a characteristic that is not present in the particular number distribution that correctly corresponds to the gamma interval distribution (see Sec. V where we provide the PND that is consistent with the gamma PID) unless a further relationship between the scaling parameter and the luminance is assumed. However, even with such a relation, the empirical PID's and PND's cannot be fitted by the theoretical curves over the entire luminance range.

Because the PND of a Poisson process having either fixed or variable dead time exhibits an increasing mean-to-variance ratio with increasing intensity,<sup>18-23</sup> a number of authors have

attempted to use a dead-time model to explain this effect. In particular, Kuffler, FitzHugh, and Barlow<sup>1</sup> considered a fixed-dead-time model, but the calculated PID (a displaced exponential) did not fit the recorded data well. Trabka,<sup>11</sup> on the other hand, attempted to incorporate a refractory period in the scaling model that Barlow and Levick<sup>6</sup> describe in order to deal with the change in increment threshold at high adaptation levels, and Rodieck<sup>4</sup> considered the effect of a stochastic dead time on the mean and standard deviation of the PID. Lee<sup>24</sup> proposed a neuronal model with stochastic dead time driven by a stationary renewal input process. Though theoretical dead-time-modified PND's have been obtained by a number of authors in various fields of endeavor,<sup>20,22,23,25,26</sup> there has been little effort in the past to use this theoretical approach to describe the distribution of nerve impulses in a discharge in general, and to describe the maintained discharge in particular.

Since we shall be developing in detail a stochastic model based on the dead-time-modified Poisson process, we give some further attention to Rodieck's previous work.<sup>4,8</sup> Rodieck's basis for considering this model lay in the observation that the relation of standard deviation and mean of the PID's for different ganglion cells was roughly linear and had a slope of unity. In each case the mean was somewhat larger than the standard deviation; the average difference was 17.0 ms with values as low as 0 ms for some units and as high as 45 ms for others. The mean and standard deviation of the PID for a Poisson process are precisely equal, but the introduction of a fixed dead time following each registered pulse (during which subsequent incoming pulses are lost) increases the mean of the PID by the value of the dead time without affecting the standard deviation. If we identify the algebraic difference between the mean and standard deviation of the empirical distributions with the dead time of such a theory, the correspondence of the data to the main properties of the dead-time-modified Poisson model is striking. In addition, dead times estimated in this way were found by Rodieck to be directly related to the time taken for the probability of a second impulse to follow a first impulse to reach half of its final value, as should be the case if the model is to hold.<sup>4</sup> This is represented by the un-normalized autocorrelelogram or postfiring interval distribution.

Most, if not all, inputs to the ganglion cell are graded and arise from cells that do not appear to exhibit refractoriness. Hence, if dead time (manifested as refractoriness) is to play a role, the ganglion cell is the most likely location at which such an influence would be exerted. This is consistent with the conclusions drawn by Rodieck<sup>4</sup> regarding the origin of the maintained discharge. Although Rodieck's finding that loss of the maintained discharge from ganglion cells consequent on chemical destruction of the photoreceptor layer implies that photoreceptors are necessary for the maintained discharge, it does not imply that the fine time structure of the discharge follows the fine time structure of the synaptic input. Instead the synaptic input may simply set a level that is appropriate to allow a ganglion cell to generate impulses. Since Rodieck<sup>4</sup> also finds that firing patterns of nearby cells may be statistically correlated, he reasons that Hughes and Maffei's<sup>27</sup> conclusion that the maintained discharge is intrinsic to the ganglion cell is not supported. Rodieck<sup>4</sup> also concludes that the synaptic input does provide a level-setting function

from the observation that the pattern of discharge following an antidromic spike is not distinguishable from that following a normally produced spike. If this is so then the generating mechanism for the fine time structure may indeed originate within the ganglion cell and would suggest even more strongly that the ganglion cell is the main—if not the only—locus in the retina at which refractoriness might play a role.

In the present work our main interest is in characterizing the stochastic properties of the maintained discharge at various fixed levels of adaptation with PND's and PID's that are consistent with each other. In addition to yielding excellent fits to the empirical stochastic distributions, the compression in sensitivity required by our model is in good accord with the experimental data and with predictions obtained from parametric feedback models<sup>28,29</sup> which characterize changes in mean response levels with adapting luminance but do not treat the stochastic properties of the maintained discharge (see also Refs. 30–35).

In Sec. II we discuss the principal bases for applying the Poisson process to the ganglion cell discharge. In Sec. III we derive the relationships between the pulse-number and pulse-interval distributions for Poisson processes with no dead-time restrictions, with a fixed dead time, and with a stochastic dead time. In Sec. IV a model is presented for the ganglion cell and the theoretical results are compared with the recorded data.<sup>5,6</sup> Section V is devoted to a discussion of the results.

## II. BASES FOR APPLICATION OF THE POISSON PROCESS TO THE GANGLION CELL DISCHARGE

Since the nerve impulse train from the single retinal ganglion cell results from the summation of a number of signals from different cells in more distal retinal layers and since, in addition, the light stimulus is effectively temporally and spatially Poisson and results in the absorption of less than one quantum per rod per millisecond under most conditions of present interest, there is some basis for considering that the Poisson process might provide a reasonable foundation for a model of the ganglion cell discharge. Limitations to the validity of this approach may be expected at high levels of adaptation where rod saturation occurs at 200–10 000 quanta absorbed per rod per second in the human,<sup>36</sup> at low levels of adaptation where absorption of one quantum may yield several nerve impulses from a single retinal ganglion cell,<sup>13</sup> and for situations in which the light is statistically different from Poisson.<sup>37</sup> In the present report our main concern shall be with data on the single cat retinal ganglion cell for a range of adapting luminances extending from a low level at which on the average one quantum is absorbed per rod every  $10^4$  s to a high level at which on the average 1000 quanta are absorbed per rod per second.

Since communication within the retina between rods, horizontal cells, amacrine cells, bipolar cells, and ganglion cells appears to be carried out almost exclusively by graded potentials rather than by pulses of fixed height, it might appear that there is some inappropriateness in developing a model that is based on pulsatile point processes. In fact, the following considerations show that this is not so: (i) If Rodieck's inference<sup>4,8</sup> (described above) is correct and the synaptic input

to the ganglion cell serves a level-setting function but does not determine the fine time structure of the maintained discharge, then whether it is pulsatile or graded is irrelevant since the pulsatile point process with which we are concerned is generated by the ganglion cell. In this case, there are no preferred time intervals so that the Poisson is the natural choice for the underlying point process generated. (ii) If, on the other hand, the fine time structure of the ganglion cell output follows its graded input, the present model incorporates it directly in the following way: Consider a system whose input consists of a stochastic series of fixed-height pulses following a Poisson distribution with mean  $M$ . The output from the first stage of this system for each input pulse is a graded potential whose height is a random variable with an arbitrary distribution. If the second stage of such a system (we call this the detector) requires an input greater than some arbitrary criterion height in order to generate an output pulse, and if the probability is  $P$  that the graded potential at the input to the detector will reach this height, then the pulse stream out of the detector will be Poisson with mean  $MP$ . Hence regardless of whether the first stage of such a system truly represents a series of compartments (e.g., rod signal is sent to a horizontal cell which itself sends a signal to a bipolar cell) and that communication from compartment to compartment within the stage is by graded potentials, regardless of whether the communication route for the signal changes (e.g., rod to bipolar on one occasion, rod to horizontal cell on another occasion), and regardless of whether a single quantum distributes signals via several pathways, as long as we can characterize the input to the detector as reaching the criterion height with some probability  $P$ , the spike stream out of the detector will be Poisson with mean  $MP$ . It is also worth noting that even if there should be a convergence of inputs to the detector, the same result would be produced, and this holds regardless of how far back from the detector is the stage at which the convergence occurred; this would also permit the dark discharge to be treated as additive with the discharge produced by quanta of light. Holden has considered a broad range of models for the generation of nerve impulses in great detail,<sup>38</sup> and the reader is referred to his book for further information.

Finally, we note an important theorem which states that the process resulting from the superposition of a number of stochastic point processes approaches the Poisson limit under a very broad range of conditions regardless of whether the point processes themselves are Poisson.<sup>39–42</sup> As first considered by McGill<sup>43</sup> the generality of this result suggests that the Poisson process may be important in neural counting mechanisms. If we consider a stochastic point process as a collection of random points, the superposition of two (or more) processes is obtained by taking the union of the points of both (or all) of the constituent processes. Perhaps the simplest and most widely known result is that the superposition of two or more independent Poisson processes is again Poisson. However, if the following four conditions are fulfilled, the superposition of a number of point processes will also approach the Poisson limit for arbitrary (not necessarily Poisson) component processes: First, we require that each of the constituent processes contribute no more than one point in the counting interval. Second, we require that the component processes be independent; since each of the  $n$  points in the process that is the result of the superposition belongs to a different component, the positions of the  $n$  points within the

counting interval are also independent. Third, we require each of the components to be stationary, so that each of the points is uniformly distributed over the counting interval. Finally, if there are  $n_T$  points in the interval  $(0, T)$  the number  $n_T$  must be such that  $n_T/T$  is the intensity or rate of the superposition process as  $T \rightarrow \infty$ . A rigorous proof of the Poisson limit was initially provided by Cox and Smith<sup>40,41</sup>; recent advances have been summarized by Çinlar.<sup>42</sup> Thus, even should the component processes giving rise to the timing of the ganglion cell's maintained discharge itself be other than Poisson, there are a broad set of conditions for which modeling the discharge with a Poisson process would provide a fair representation.

### III. RELATION BETWEEN PULSE-NUMBER AND PULSE-INTERVAL DISTRIBUTIONS

We now consider the relationship between various pulse-number distributions and the corresponding pulse-interval distributions.<sup>17,19,23,44</sup> First we obtain an expression relating the PND and the PID for the Poisson process in the absence of dead-time restrictions. (For a nonparalyzable counter, the dead time represents a period of time, after the registration of a pulse, during which other pulses are not registered, and furthermore, do not prolong the duration of the dead-time period.) We then obtain the relationship in the presence of fixed dead time,<sup>22,23,25,26</sup> finally generalizing this to allow for a stochastic dead time.<sup>24,45-47</sup> An exact expression for the PID and an approximate expression for the PND is obtained when the variation in dead time can be represented by a Gaussian distribution. Relevant examples are presented to illustrate each of the situations considered.

#### A. Absence of dead time

Consider the Poisson pulse-number distribution  $p(n, t)$  representing, for each integer  $n$ , the probability of registering  $n$  pulses in a time interval  $t$ . We seek an expression for the pulse-interval distribution of the underlying process in terms of the pulse-number distribution. Let  $F(t)$  represent the probability that the arrival time of the succeeding pulse is  $\leq t$  following the registration of a pulse at time  $t = 0$ . Clearly,  $F(t)$  is the cumulative probability distribution of the pulse-interval density, denoted by  $f(t)$ , i.e.,

$$F(t) = \int_0^t f(t') dt'. \quad (1)$$

By definition, only arrival times  $t \geq 0$  are considered. Equivalently,  $1 - F(t)$  is the probability that the arrival of the next pulse occurs after time  $t$ , i.e., that exactly zero events occur in the interval  $(0, t)$ . Therefore,

$$1 - F(t) = p(0, t), \quad (2)$$

which, when combined with Eq. (1), yields

$$1 - \int_0^t f(t') dt' = p(0, t). \quad (3)$$

Differentiation of Eq. (3) with respect to  $t$  yields the desired relationship,

$$f(t) = -\partial p(0, t)/\partial t. \quad (4)$$

Thus for a Poisson process with mean rate  $\lambda$ , the PND is given by

$$p(n, T) = (\lambda T)^n \exp(-\lambda T)/n!, \quad (5)$$

so that the probability of registering zero counts in the time interval  $T$  is

$$p(0, T) = \exp(-\lambda T), \quad (6)$$

where  $0! \equiv 1$ . The corresponding PID is obtained by differentiation of Eq. (6), in accordance with Eq. (4), i.e.,

$$f(t) = \lambda \exp(-\lambda t). \quad (7)$$

This is the familiar exponential distribution.<sup>17,19,48</sup>

Processes other than Poisson, e.g., those with nonindependent pulses such as the strictly periodic pulse train<sup>12</sup> or the doubly-stochastic Poisson process,<sup>37</sup> must be treated more carefully. In general, a distinction must be made between the density function for interspike intervals (PID) and the density function for the time to the first pulse with the time origin chosen arbitrarily (first time-of-arrival or time-interval distribution, denoted TID).<sup>17,44,49,50</sup> Indeed, for a particular (experimental or theoretical) TID it is in principle possible, by repeated differentiation of the TID, to obtain an estimate of the PND. The TID may also be expressed as a sum over a set of PND's, though the accuracy of these relations is limited in practice (see Ref. 17, pp. 106-108). Dead-time effects further complicate the interrelation. The Poisson process is sufficiently general to meet our needs, however, in which case no distinction need be made between the PID and the TID.

#### B. Fixed dead time

We now consider a random Poisson pulse train at the input to a processor. The output of this processor is defined to be identical to the input, with the restriction that following each output pulse, there is a (nonparalyzable) dead time  $\tau$  during which no further output pulses can occur. At the termination of the dead time, the processor is again free to respond to incoming pulses. We investigate the PID at the output of the processor, i.e., the dead-time-modified pulse-interval distribution. For a Poisson input process the pulses are independent, i.e., the probability of occurrence of a given pulse does not depend on the occurrence or nonoccurrence of previous pulses. For this reason, the Poisson process is sometimes called a purely random or zero-memory process.<sup>48</sup> Furthermore, the exponential pulse-interval distribution [see Eq. (7)] has the following property: Beginning at any time  $t_0$ , the probability of the next pulse occurring at time  $t \geq t_0$  is given by

$$f(t) = \lambda \exp[-\lambda(t - t_0)] \quad t \geq t_0. \quad (8)$$

The pulse-interval distribution for a Poisson process with fixed dead time  $\tau$  is therefore<sup>1,4,19,24,25</sup>

$$f(t|\tau) = \lambda \exp[-\lambda(t - \tau)] \quad t \geq \tau. \quad (9)$$

Thus at the termination of the dead time which follows a given pulse, the process behaves as if this time interval did not exist (has no memory) and the PID for the dead-time-modified process is obtained by simply replacing  $t$  by  $t - \tau$  (for  $t \geq \tau$ ) in the unmodified PID.

For a Poisson process with fixed dead time  $\tau$ , the probability of registering  $n$  counts in a time interval  $T$  (PND) with a nonparalyzable counter is<sup>22,23,25</sup>

$$p(n, T|\tau) = \begin{cases} e^{-\lambda T}, & n = 0 \\ \sum_{k=0}^n \{\lambda^k [T - n\tau]^k / k!\} \exp\{-\lambda[T - n\tau]\} & \\ - \sum_{k=0}^{n-1} \{\lambda^k [T - (n-1)\tau]^k / k!\} \exp\{-\lambda[T - (n-1)\tau]\}, & 1 \leq n < T/\tau \\ 1 - \sum_{k=0}^{n-1} \{\lambda^k [T - (n-1)\tau]^k / k!\} \exp\{-\lambda[T - (n-1)\tau]\}, & T/\tau \leq n < (T/\tau) + 1 \end{cases} \quad (10)$$

assuming that a pulse did not occur just prior to the beginning of the sampling interval (unblocked or free counter). Count numbers greater than  $(T/\tau) + 1$  are forbidden. Figure 2 shows the deviation from the original Poisson PND when the effects of dead time are included, and also provides a comparison with a normalized (mean approximately equal to that of the original Poisson) dead-time-modified PND.<sup>23</sup> The ratio of dead time to sampling time  $\tau/T = 0.025$  for all curves. The mean of the original Poisson (solid curve) along with its variance was set equal to 25.0; it can be seen from Fig. 2 that the mean of the dead-time-modified PND (dotted curve) is reduced to 16.3, whereas its variance is reduced to 5.6. The dashed curve was obtained by increasing  $\lambda T$  to 66.5 from  $\lambda T = 25$  in order to approximately compensate for dead-time losses in the mean. This clearly demonstrates the reduction in variance (= 3.6) due to dead-time effects. These effects become more pronounced with increasing values of  $\tau/T$ . It is worth noting that the parameters yielding the substantial effects in Fig. 2 are equivalent to a refractory period (dead time) of 1.25 ms with a sampling interval of duration 50 ms, values that would be appropriate in the physiological range. The asymptotic mean and variance for the dead-time-modified PND are given explicitly by<sup>18-23</sup>

$$\bar{n} \simeq \lambda T(1 + \lambda\tau)^{-1} + \frac{1}{2}(\lambda\tau)^2(1 + \lambda\tau)^{-2} \quad (11)$$

and

$$\sigma^2 \simeq \lambda T(1 + \lambda\tau)^{-3}, \quad (12)$$

respectively. Note that the second term in Eq. (11),  $\frac{1}{2}(\lambda\tau)^2 \times (1 + \lambda\tau)^{-2}$ , is always  $< \frac{1}{2}$  (for  $\tau > 0$ ), so we may just as well write

$$\bar{n} \simeq \lambda T(1 + \lambda\tau)^{-1}. \quad (13)$$

In fact, Müller<sup>22</sup> has shown that Eq. (13) represents the exact as well as the asymptotic mean for the equilibrium process, representing a random choice of time origin rather than the particular choice corresponding to an unblocked (free) counter. Furthermore, Eq. (12) represents a good approximation for the asymptotic variance of the equilibrium process as well as for the shifted process (unblocked counter). Using the terminology of renewal theory, we note that this section has dealt with a quasi-Poisson process,<sup>51,52</sup> as is clear from the form of the renewal function  $\bar{n}$  represented in Eqs. (11) and (13). Finally, we observe that since  $\lambda T$  is the average number of pulses that would be registered in the sampling time  $T$  in the absence of dead time, the ratio  $\bar{n}/\lambda T \simeq (1 + \lambda\tau)^{-1}$  [see Eq. (13)] represents the fractional transmission of the dead-time processor.

### C. Variable-dead-time PID

We now consider a dead time that is not fixed, but that undergoes random variations.<sup>24,45-47</sup> This model has been discussed by Rodieck<sup>4,8</sup> in relation to the maintained discharge considered here. We note that the dead time imposed by a multichannel analyzer used in nuclear event measurements is also generally random.<sup>21</sup> In both of these cases, the stochastic dead-time variations can be represented in terms of a probability distribution  $P(\tau)$ , assumed to be statistically independent of the input process and to have mean value  $\bar{\tau}$  and variance  $\sigma_\tau^2$ . It is shown in Appendix A that the exact pulse-interval distribution for a Poisson process with a Gaussian-distributed dead time is [see Eq. (A8)]

$$f(t) = \frac{\lambda}{2} \left[ \exp - \left( \lambda(t - \bar{\tau}) - \frac{(\sigma_\tau \lambda)^2}{2} \right) \right] \left[ \frac{1}{2} \operatorname{erfc} \left( \frac{-\bar{\tau}}{2^{1/2} \sigma_\tau} \right) \right]^{-1} \times \left[ \operatorname{erfc} \left( -\frac{t - \bar{\tau} - \sigma_\tau^2 \lambda}{2^{1/2} \sigma_\tau} \right) - \operatorname{erfc} \left( \frac{\bar{\tau} + \sigma_\tau^2 \lambda}{2^{1/2} \sigma_\tau} \right) \right], \quad (14)$$

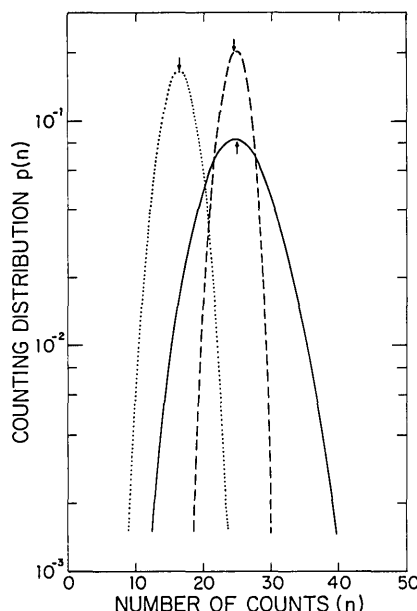


FIG. 2. The Poisson theoretical pulse-number distribution with no dead time is represented by the solid curve (mean = variance = 25.0). The effects of dead time produce the theoretical pulse-number distribution shown by the dotted curve (mean = 16.3, variance = 5.6). The dead-time-modified theoretical PND normalized to approximately the same mean as the unmodified Poisson distribution is shown by the dashed curve (mean = 24.6, variance = 3.6). The ratio of dead time to sampling time  $\tau/T$  was chosen to be 0.025 for all curves. Arrows indicate means. After Cantor and Teich (Ref. 23).

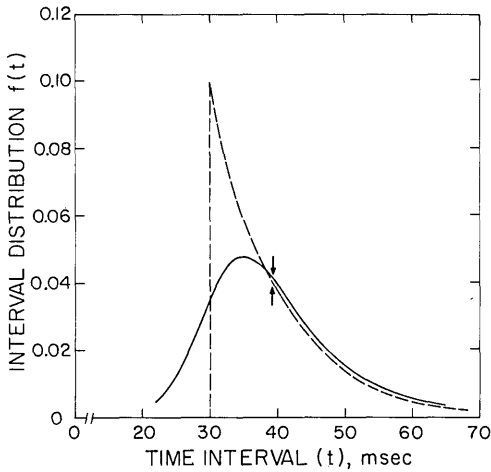


FIG. 3. Theoretical pulse-interval distributions for fixed (dashed curve) and variable (solid curve) dead time. For the dashed curve, the dead time  $\tau$  was chosen to be 30.0 ms as was the mean dead time  $\bar{\tau}$  used in obtaining the solid curve. The dead-time variance  $\sigma_\tau^2$  was taken to be 25.0 ms<sup>2</sup> (solid curve), and the rate parameter  $\lambda$  was taken as 0.1 ms<sup>-1</sup> for both curves. Note the substantial change in shape due to the dead-time variation. Means are indicated by arrows.

where  $\text{erfc}x$  is the complementary error function<sup>53</sup> evaluated at  $x$ .

This distribution is plotted in Fig. 3 for  $\bar{\tau} = 30.0$  ms and  $\sigma_\tau^2 = 25.0$  ms<sup>2</sup> (solid curve). Note the considerable difference in shape (arising from the dead-time variation) in comparison with the fixed-dead-time PID with  $\tau = 30.0$  ms (dashed curve), which is simply a displaced exponential. Both curves correspond to a value  $\lambda = 0.1$  ms<sup>-1</sup>.

#### D. Variable-dead-time PND

To obtain the corresponding pulse-number distribution, we use a generalized expression for the fixed dead-time-modified distribution to include the case in which the dead times following the occurrences of different pulses may take on different values. Specifically, the first pulse is assumed to be followed by dead time  $\tau_1$ , the second by  $\tau_2$ , and so on up to the  $n$ th pulse, which is followed by dead time  $\tau_n$ . For a nonparalyzable counter unblocked at the beginning of the counting interval, this distribution is given by<sup>54</sup>

$$\begin{aligned}
 p(n, T | \tau_1, \tau_2, \dots, \tau_n) &= \sum_{k=0}^n \{ \lambda^k [T - (\tau_1 + \tau_2 + \dots + \tau_n)]^k / k! \} \\
 &\times \exp\{-\lambda [T - (\tau_1 + \tau_2 + \dots + \tau_n)]\} \\
 &- \sum_{k=0}^{n-1} \{ \lambda^k [T - (\tau_1 + \tau_2 + \dots + \tau_{n-1})]^k / k! \} \\
 &\times \exp\{-\lambda [T - (\tau_1 + \tau_2 + \dots + \tau_{n-1})]\}, \quad n \geq 1 \quad (15)
 \end{aligned}$$

for  $T > \tau_1 + \tau_2 + \dots + \tau_n$ . Assuming each of the dead times  $\tau_i$  to be an independent sample of the underlying Gaussian random variation of the dead time, it is shown in Appendix B that to good approximation the PND is [see Eqs. (B13) and (B14)]

$$p(n, T, \bar{\tau}, \sigma_\tau) \simeq \sum_{k=0}^n p_{k,n} - \sum_{k=0}^{n-1} p_{k,n-1}, \quad n \geq 1 \quad (16)$$

where

$$\begin{aligned}
 p_{k,n} \simeq \frac{1}{2} [\lambda^{2^{1/2} n^{1/2} \sigma_\tau}]^k \exp\{-\lambda [T - n\bar{\tau}] - \frac{1}{2} n \sigma_\tau^2 \lambda^2\} \\
 \times i^k \text{erfc}\{-(T - n\bar{\tau} - n\lambda \sigma_\tau^2) (2^{1/2} n^{1/2} \sigma_\tau)^{-1}\}. \quad (17)
 \end{aligned}$$

Here  $i^k \text{erfc}x$  represents the  $k$ th iterated integral of the complementary error function<sup>53</sup> evaluated at  $x$ .

In Fig. 4 we present plots of the PND represented by Eqs. (16) and (17) for two different values of the dead-time variance  $\sigma_\tau^2$  in order to illustrate the effect of this parameter on the distributions. The mean number of counts  $\bar{n} = 3.0$  and the mean dead time  $\bar{\tau} = 10.0$  ms for both plots; the rate parameter  $\lambda$  was set equal to 0.04197 ms<sup>-1</sup> and the counting interval  $T$  was chosen as 100 ms for both distributions. The dead-time variance  $\sigma_\tau^2$  was set at 0.1 ms<sup>2</sup> (solid lines) and 50.0 ms<sup>2</sup> (dashed lines). The resulting variances of the two counting distributions are quite similar, viz.,  $\sigma^2 = 1.54$  (solid lines) and  $\sigma^2 = 1.70$  (dashed lines). Thus the dead-time variance has little effect on the counting distribution in this example. In all cases throughout this paper, the dead-time distributions  $P(\tau)$  are reasonably narrow (i.e.,  $\bar{\tau} > \sigma_\tau$ ); it is therefore expected that the fixed-dead-time PND can be used in place of the variable-dead-time expression. It is of interest to note that for  $\bar{n} < 1$ , the effect on the PND of dead-time variability is expected to be substantial since the PID, which is related to the probability of  $n = 0$  through Eq. (A2), is sensitive to this variation.

#### E. PND mean-to-variance ratio

In the absence of dead time, the mean  $\bar{n}_P$  and variance  $\sigma_P^2$  of a Poisson process with mean rate  $\lambda$  [see Eq. (5)] are equal, viz.,

$$\bar{n}_P = \sigma_P^2 = \lambda T. \quad (18)$$

For a fixed-dead-time-modified Poisson process, expressions for the asymptotic mean and variance are given by Eqs.

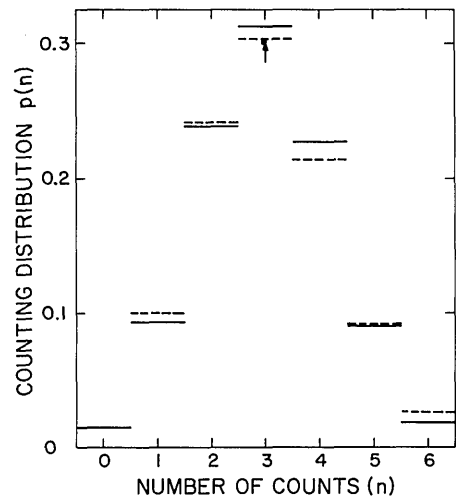


FIG. 4. Theoretical pulse-number distributions for a variable-dead-time-modified Poisson distribution. The solid lines (mean = 3.0, variance = 1.54) represent a (small) dead-time variance  $\sigma_\tau^2 = 0.1$  ms<sup>2</sup> and a mean dead time  $\bar{\tau} = 10.0$  ms. The dashed lines (mean = 3.0, variance = 1.70) represent a (relatively large) dead-time variance  $\sigma_\tau^2 = 50.0$  ms<sup>2</sup> and the same mean dead time  $\bar{\tau} = 10.0$  ms. The counting interval  $T$  was taken equal to 100 ms and the rate parameter  $\lambda$  was 0.04197 ms<sup>-1</sup> for both cases. The mean count is indicated by an arrow. At  $n = 0$ , the two lines coincide since the counter is assumed to be unblocked.

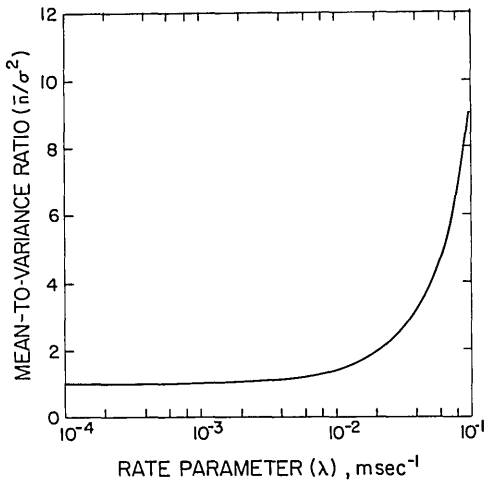


FIG. 5. The mean-to-variance ratio of the dead-time-modified Poisson theoretical PND as a function of the logarithm of the rate parameter  $\lambda$ . The dead time  $\tau$  is 20.0 ms.

(11)–(13). Using Eqs. (12) and (13), the ratio of mean to variance for a fixed dead time  $\tau$  is, to good approximation, a parabola in  $\lambda$  for fixed  $\tau$ , i.e.,

$$\bar{n}/\sigma^2 \approx (1 + \lambda\tau)^2. \quad (19)$$

Since the approximation represented by Eq. (19) is applicable for the equilibrium process as well as for the shifted process (free counter),<sup>22</sup> the unblocked nature of our results is not critical in this context. Furthermore, the dead-time variance has little effect on the PND's for all cases considered here so that the mean-to-variance ratio will be approximately the same as that for a fixed dead time equal to the mean dead time  $\bar{\tau}$ . Figure 5 shows a plot of this function for  $\tau = 20.0$  ms with  $\lambda$  ranging from  $10^{-4}$  to  $10^{-1}$   $\text{ms}^{-1}$  on a logarithmic scale.

To this point we have obtained a number of expressions for pulse-number and pulse-interval distributions in the absence of dead time, for fixed dead time, and for variable dead time. These results, in conjunction with the experimental distributions measured by Barlow and Levick,<sup>5,6</sup> are used in the next section to provide a model for the statistical behavior of the all-or-none maintained discharge in the retinal ganglion cell of the cat.

#### IV. GANGLION CELL MODEL AND COMPARISON WITH DATA

The theoretical results obtained in the last section are now applied to the experimental pulse-number and pulse-interval distributions of the maintained discharge recorded from the retinal ganglion cell of the cat.<sup>5,6</sup> As mentioned earlier, attempts to use a fixed-dead-time model<sup>1</sup> were unsatisfactory inasmuch as the theoretical PID's did not fit the data. Theoretical dead-time-modified PND's, which are far less sensitive to the details of the dead time, were not available until recently.<sup>22,23,25,26</sup> As a result, considerations of refractoriness were, with few exceptions,<sup>4,8</sup> given less attention than scaling models. The latter, which give rise to gamma pulse-interval distributions, generally fit the data far better than do the fixed-dead-time PID's, but with parameters that are improper.<sup>6,9</sup> This will be discussed in more detail in the next

section. The stochastic-dead-time model, as we now show, provides consistent and reasonable fits for both the pulse-number and pulse-interval distributions.

A schematic representation is given in Fig. 6: The ganglion cell may be viewed as the locus of a union of the point processes that result, at its *output*, from individual excitation signals. Lines A, B, and C in Fig. 6 each indicate the ganglion cell *output* due to an exclusive excitation (e.g., by a bipolar cell). In actuality, there will be many more than three inputs to a given ganglion cell. Using the results of Sec. II, we infer that the process that is the union of the outputs due to a number of excitations (line D in Fig. 6) approaches Poisson (with rate parameter  $\lambda$ ) for luminance values sufficiently large that bunching effects<sup>13</sup> are negligible. Alternatively, we note that the stochastic time course of the pulse train may be generated wholly within the ganglion cell itself, in which case the details of the pulse train do not in any way reflect the time course at the input to the ganglion cell. Our model makes no predictions on this point but rather provides an adequate representation for both realizations.

In either case, the overall process (line D) is assumed to be Poisson and subject to the restrictions of a stochastic non-paralyzable dead time, inasmuch as the ganglion cell itself requires time to recover after the registration of a pulse. The output process (line E in Fig. 6) then consists of a stochastic-dead-time-limited point process; the values of the dead time denoted by  $\tau_1, \tau_2, \dots, \tau_8$  represent samples of the dead-time random variable.

As discussed previously, we use a Gaussian distribution to model the variation in dead time. This distribution yields results similar to those obtainable using any singly peaked continuous probability density. It is truncated at  $\tau = 0$  when computing the PID. The PID and PND for this process were presented in Eqs. (14), (16), and (17); the experimental data will be fit with these distributions using suitably chosen values of the dead-time mean and variance,  $\bar{\tau}$  and  $\sigma_\tau^2$ , respectively.

In Figs. 7–10 we present a number of (best visual) theoretical fits to Barlow and Levick's<sup>6</sup> experimental data. For an observed mean count  $\bar{n}$  in a prescribed counting interval  $T$ , the rate parameter  $\lambda$  was determined from the expression

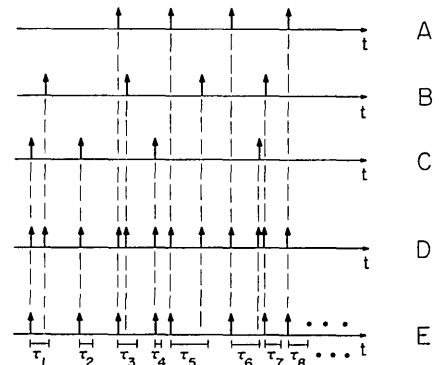


FIG. 6. Schematic representation of a set of sample functions for the ganglion cell model. Lines A, B, and C represent hypothetical *outputs* due to individual excitations (e.g., each line may represent the response to a single bipolar cell). Line D represents the union of the three processes A, B, and C. Line E shows the variable dead time effect on this union, and represents the ganglion cell output. The quantities  $\tau_1, \tau_2, \dots, \tau_8$  represent samples of the stochastic dead time.

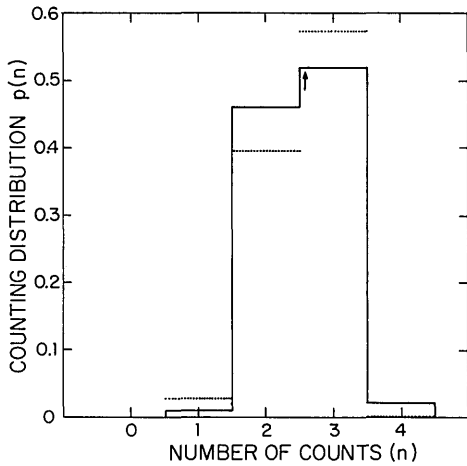


FIG. 7. Experimental PND (stepped histogram, 1000 samples) and theoretical fixed-dead-time PND (dotted lines) for an on-center unit at a luminance of 3.4 cd/m<sup>2</sup>. The dead time  $\tau$  is 31.0 ms, the rate parameter  $\lambda$  is 0.0787 ms<sup>-1</sup>, and the counting interval  $T$  is 100 ms. Arrow indicates mean number of counts. Data adapted from Fig. 5 of the paper by Barlow and Levick (Ref. 6).

$$\bar{n} \approx \lambda T(1 + \lambda \bar{\tau})^{-1} + \frac{1}{2}(\lambda \bar{\tau})^2(1 + \lambda \bar{\tau})^{-2}, \quad (20)$$

where  $\bar{\tau}$  is the mean dead time yielding the best fit. This approximate determination of the parameter  $\lambda$  turns out to be sufficiently accurate so that the more complicated expression including  $P(\tau)$  need not be used. Both the pulse-number and pulse-interval distributions are determined from a single set of parameters  $\lambda$ ,  $\bar{\tau}$ , and  $\sigma_{\tau}^2$ . Formal curve-fitting procedures were not used so that better fits than those presented here could presumably be obtained.

Figures 7 and 8 show the theoretical distributions along with the recorded data for an ordinary on-center unit at a luminance of 3.4 cd/m<sup>2</sup>, whereas Figs. 9 and 10 correspond to an off-center unit at the same luminance. In Fig. 7 the theoretical distribution is shown by the dotted lines, whereas in Figs. 8–10 the theoretical results are shown as smooth curves.

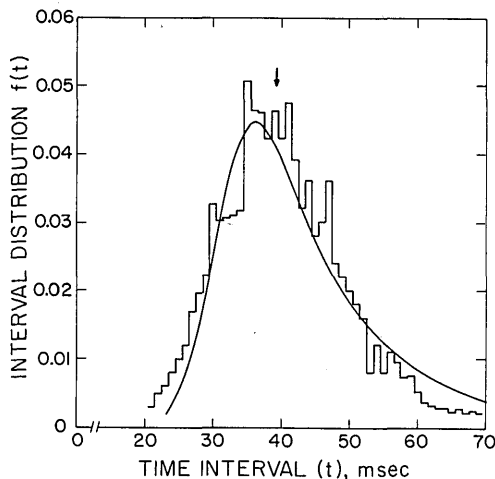


FIG. 8. Experimental PID (stepped histogram, 2000 intervals) and theoretical PID (smooth curve) corresponding to the on-center unit of Fig. 7. The parameters  $\bar{\tau}$ ,  $\sigma_{\tau}^2$ , and  $\lambda$  are again 31.0 ms, 18.0 ms<sup>2</sup>, and 0.0787 ms<sup>-1</sup>, respectively. Note that the mean dead time is the same as the (fixed) dead time used in the PND. Arrow indicates mean time interval. Data adapted from Fig. 5 of the paper by Barlow and Levick (Ref. 6).

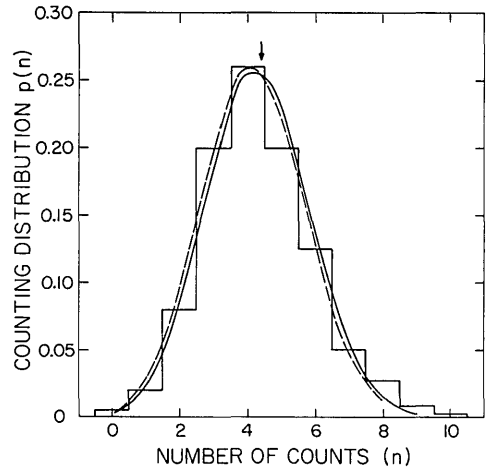


FIG. 9. Experimental PND (stepped histogram, 1000 samples) and theoretical variable-dead-time PND (solid curve) for an off-center unit at a luminance of 3.4 cd/m<sup>2</sup>. The mean dead time  $\bar{\tau}$  is 6.5 ms, the dead-time variance  $\sigma_{\tau}^2$  is 3.24 ms<sup>2</sup>, and the rate parameter  $\lambda$  is 0.0589 ms<sup>-1</sup>. The dashed curve corresponds to the theoretical fixed-dead-time PND with  $\tau = 6.5$  ms and the same value of  $\lambda$ . The counting interval  $T$  is 100 ms for all curves. Arrow indicates mean number of counts. Data adapted from the paper by Barlow and Levick (Ref. 6).

In all cases, the stepped histograms represent data adapted from Fig. 5 of the paper by Barlow and Levick.<sup>6</sup> No attempt was made to draw a continuous curve for the theoretical results of Fig. 7 since there are so few points and the number distribution is, of course, discrete. Smooth curves were used in Fig. 9 only for simplicity.

For the on-center unit represented in Figs. 7 and 8, the parameters used are  $\lambda = 0.0787$  ms<sup>-1</sup>,  $\bar{\tau} = 31.0$  ms, and  $\sigma_{\tau}^2 = 18.0$  ms<sup>2</sup> for the PID, and  $\tau = 31.0$  ms,  $T = 100$  ms and  $\lambda = 0.0787$  ms<sup>-1</sup> for the PND. For the off-center unit represented in Figs. 9 and 10, the parameters are  $T = 100$  ms,  $\lambda = 0.0589$  ms<sup>-1</sup>,  $\bar{\tau} = 6.5$  ms, and  $\sigma_{\tau}^2 = 3.24$  ms<sup>2</sup> for both the PID and PND. The fits obtained are very good. We note that Barlow and Levick<sup>6</sup> were unable to obtain a satisfactory fit to the recorded interval distribution for the off-center unit (Fig. 10) using the

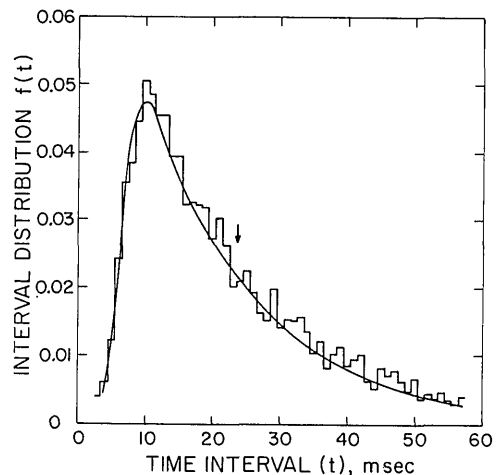


Fig. 10. Experimental PID (stepped histogram, 4000 intervals) and theoretical PID (smooth curve) corresponding to the off-center unit of Fig. 9. The parameters  $\bar{\tau}$ ,  $\sigma_{\tau}^2$ , and  $\lambda$  are again 6.5 ms, 3.24 ms<sup>2</sup>, and 0.0589 ms<sup>-1</sup>, respectively. Arrow indicates mean time interval. Data adapted from the paper by Barlow and Levick (Ref. 6).

gamma (also known as the Erlang or Pearson type III) density with which they attempted to model the PID.

It has been shown earlier (see Fig. 4) that the variation in dead time has little effect on the pulse-number distribution. This fact, coupled with the computational difficulties encountered in evaluating the PND in Eqs. (16) and (17) for high count numbers  $n$  and in cases where the dead time is large, has encouraged us to use the (much simpler) fixed-dead-time PND [see Eq. (10)] as a good approximation. The dead time  $\tau$  used in the pulse-number distribution is set equal to the mean dead time  $\bar{\tau}$  used in the pulse-interval distribution [see Eq. (14)]. In Fig. 7 the fixed-dead-time PND (dotted lines) is seen to provide a reasonably good fit to the observed distribution (stepped histogram). In Fig. 9 the fixed-dead-time (dashed curve) and the variable-dead-time (solid curve) theoretical PND's are compared with the recorded data to clearly illustrate this point. Recall that in calculating all PND's, it has been assumed that the ganglion cell is unblocked at the beginning of each counting interval. This assumption is important only at very low count numbers, such as those encountered in Fig. 7. The equilibrium process counting distribution calculated by Müller<sup>22</sup> would likely provide a better fit to the data, since for an initially blocked counter, there is essentially one more dead time present in the interval. This would tend to decrease the probability at  $n = 3$  in Fig. 7, providing an even better fit to the data. This effect can be ignored in Fig. 9.

Figures 11–14 present comparisons of the theoretical distributions with the recorded data for an (on-center) luminance unit (II:2) and another "ordinary" on-center unit (DD:6), as adapted from Fig. 10 of the paper by Barlow and Levick.<sup>6</sup> The luminance unit, if it can be classified as a separate type at all<sup>6</sup> is rare and is characterized by a mean firing rate that closely follows the adapting luminance. Furthermore, pulses from these units are far more regular than those recorded from either on-center or off-center units. The theoretical PND in Fig. 11 is plotted for a (fixed) dead time with  $\tau = 24.5$  ms,  $T = 1000$  ms, and  $\lambda = 0.148$  ms<sup>-1</sup>, whereas the interval distribution in Fig. 12 has a mean dead time  $\bar{\tau} = 24.5$  ms, a dead-

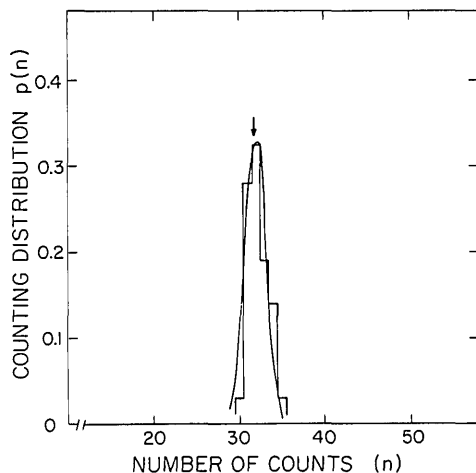


FIG. 11. Experimental PND (stepped histogram, 100 samples) for a luminance unit at 3.4 cd/m<sup>2</sup>. The smooth curve is the fixed-dead-time ( $\tau = 24.5$  ms) theoretical PND, with rate parameter  $\lambda = 0.148$  ms<sup>-1</sup> and counting interval  $T = 1000$  ms. Arrow indicates mean. Data adapted from Fig. 9 of the paper by Barlow and Levick (Ref. 6).

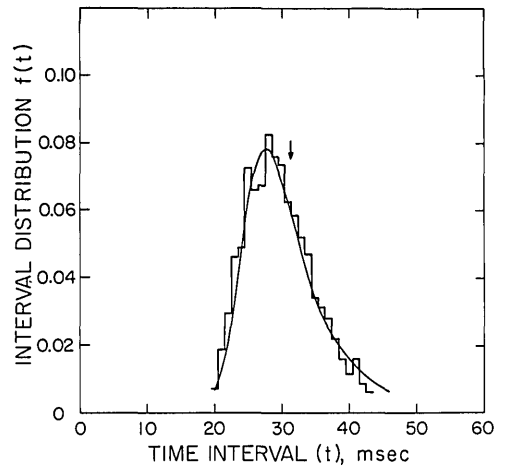


FIG. 12. Experimental PID (stepped histogram, 3003 intervals) corresponding to the luminance unit of Fig. 11. The theoretical PID (smooth curve) has a mean dead time  $\bar{\tau} = 24.5$  ms and dead-time variance  $\sigma_{\tau}^2 = 7.56$  ms<sup>2</sup> with a rate parameter  $\lambda = 0.148$  ms<sup>-1</sup>, as in Fig. 11. Again, the mean dead time is taken equal to the (fixed) dead time used in the PND. Arrow indicates mean time interval. Data adapted from Fig. 9 of the paper by Barlow and Levick (Ref. 6).

time variance  $\sigma_{\tau}^2 = 7.56$  ms<sup>2</sup>, and again  $\lambda = 0.148$  ms<sup>-1</sup>. The data were recorded at an adaptation level of 3.4 cd/m<sup>2</sup>. It is clear that the PND and PID obtained from the stochastic dead-time model fit the luminance unit data well. In Fig. 13 the counting distribution for on-center unit DD:6 is plotted for a (fixed) dead time  $\tau = 10.0$  ms, with  $T = 1000$  ms and  $\lambda = 0.110$  ms<sup>-1</sup>. The corresponding pulse-interval distribution is shown in Fig. 14 with mean dead time  $\bar{\tau} = 10.0$  ms, dead-time variance  $\sigma_{\tau}^2 = 45.0$  ms<sup>2</sup> and, again,  $\lambda = 0.110$  ms<sup>-1</sup>. The fixed-dead-time PND does not appear to provide a good fit in Fig. 13, this being the only such case we have found; we note, however, that the experimental results represent only 100 samples. The recorded interval distribution in Fig. 14, on the other hand, represents over 5000 intervals, and is fit well by the theoretical PID. It is interesting to compare Fig. 14 with Fig. 8 inasmuch as they both represent PID's for (different)

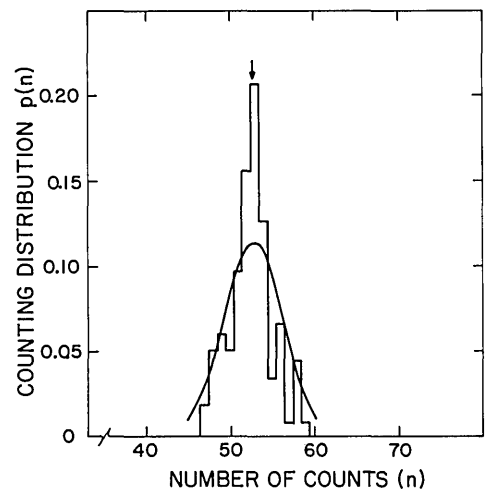


FIG. 13. Experimental and theoretical PND's for another on-center unit. Again, the fixed dead-time ( $\tau = 10.0$  ms) theoretical result (smooth curve) is used. The rate parameter  $\lambda$  is 0.110 ms<sup>-1</sup> and the counting interval  $T$  is 1000 ms. The data was recorded at an adaptation level of 3.4 cd/m<sup>2</sup> and is shown as the stepped histogram (100 samples). Arrow indicates mean. Data adapted from Fig. 9 of the paper by Barlow and Levick (Ref. 6).

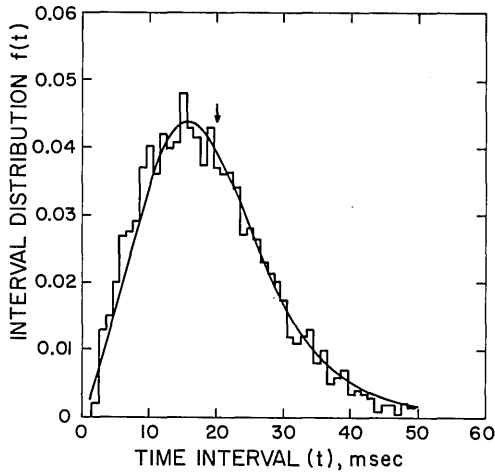


FIG. 14. Experimental PID (stepped histogram, 5007 intervals) and theoretical PID (smooth curve) corresponding to the on-center unit of Fig. 13. The parameters  $\bar{\tau}$ ,  $\sigma^2$ , and  $\lambda$  are 10.0 ms, 45 ms<sup>2</sup>, and 0.110 ms<sup>-1</sup>, respectively. Note that the mean dead time is taken equal to the (fixed) dead time used in the PND. Arrow indicates mean time interval. Data adapted from Fig. 9 of the paper by Barlow and Levick (Ref. 6).

on-center units at the same adaptation level; the parameters describing their behavior are, nevertheless, quite different.

For fixed luminance, Barlow and Levick<sup>5</sup> found the variance of the pulse-number distribution to be approximately proportional to the counting interval  $T$ . The fixed-dead-time PND, in fact, has precisely this characteristic [see Eq. (12)], as does the Poisson distribution [see Eq. (18)], the scaled Poisson distribution presented in the next section [see Eq. (24)], and the paralyzable counter also presented in the next section [see Eq. (25b)]. Figure 15 shows the theoretical curve (solid line) obtained by using the data at  $T = 0.6$  s to compute values for the parameters  $\lambda$  and  $\tau$  from Eqs. (12) and (13); also

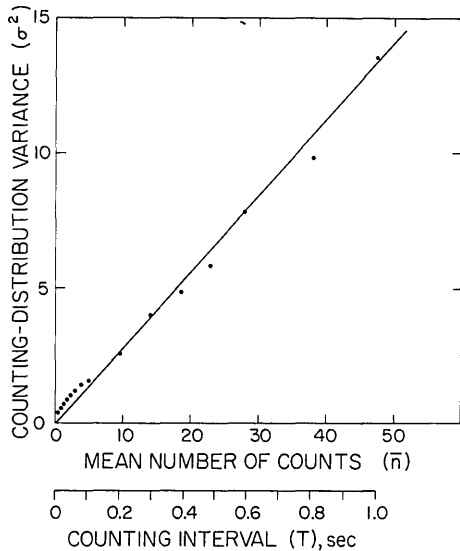


FIG. 15. The variance  $\sigma^2$  of the experimental PND (individual points) is plotted as a function of the counting interval  $T$  and, by consequence, the mean count  $\bar{n}$ . The fixed-dead-time theoretical result is shown as the straight line and was obtained by using Eq. (12) with  $\tau = 9.835$  ms and  $\lambda = 0.089$  ms<sup>-1</sup>. The data was obtained at an adapting luminance of 40 cd/m<sup>2</sup>. Data adapted from Fig. 4 of the paper by Barlow and Levick (Ref. 5).

shown are the recorded data adapted from Fig. 4 of the paper by Barlow and Levick<sup>5</sup> for this on-center unit at a (high) luminance of 40 cd/m<sup>2</sup>. The stepped histograms in Figs. 16–19 represent the actual recorded PND's for  $T = 40, 100, 400,$  and 1000 ms, respectively, as adapted from Fig. 3 of the paper by Barlow and Levick.<sup>5</sup> The theoretical distributions are shown as dashed lines in Figs. 16 and 17 and as smooth curves in Figs. 18 and 19. The (fixed) average dead time  $\tau$  and the rate parameter  $\lambda$  were set equal to 9.835 ms and 0.089 ms<sup>-1</sup>, respectively, for all theoretical curves. The fits for all cases (Figs. 15–19) are seen to be very good, indicating that the  $T$ -dependence of the dead-time model is appropriate.

Barlow and Levick<sup>6</sup> found, furthermore, that the mean-to-variance ratio of the pulse-number distribution for most on-center units generally increased with increasing luminance, which is linked to the rate parameter  $\lambda$ . We have seen previously (Fig. 5) that the dead-time-modified Poisson distribution exhibits similar behavior, although it cannot predict all of the experimental data with a single set of values for the parameters  $\lambda$  and  $\tau$ . We can, however, use the experimental data presented in Fig. 6 of the paper by Barlow and Levick<sup>6</sup> for the mean number of counts and for the mean-to-variance ratio for a single on-center unit (DD:6) to obtain unique values of  $\lambda$  and  $\tau$  as a function of luminance. Using the fixed-dead-time approximations for the mean and for the mean-to-variance ratio given in Eqs. (13) and (19), respectively, we obtain the results presented in Table I and shown in Fig. 20. Since Eq. (19) is applicable only for mean-to-variance ratios  $\geq 1$ , and ignores the bunching effects observed by Barlow, Levick, and Yoon<sup>13</sup> at low luminance levels (which they interpret as a consequence of a single quantum yielding several impulses in a ganglion cell), we have shifted the mean-to-variance ratio up by about  $1/2$  to yield a minimum mean-to-variance ratio equal to 1. This procedure does not disturb the data in any significant way and is equivalent to the clustering of impulses in groups of 2 or 3 at low luminance levels to theoretically eliminate multiplication effects and restore Poisson behavior as performed in Fig. 5 of the paper by Barlow, Levick, and Yoon.<sup>13</sup> It is interesting to note, in any case, that the

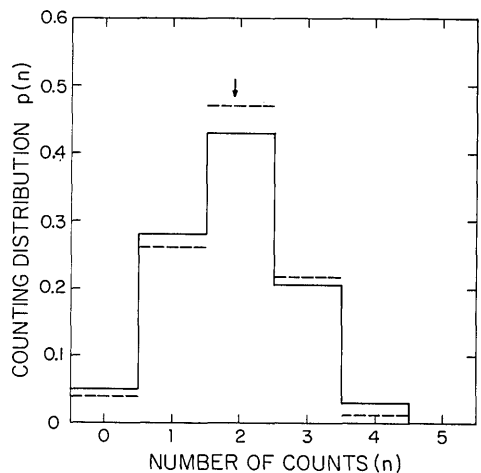


FIG. 16. Experimental PND (stepped histogram, 10 000 samples) and theoretical fixed-dead-time PND (dashed lines) for an on-center unit at a background of 40 cd/m<sup>2</sup>. This corresponds to one data point in Fig. 15, for  $T = 40$  ms,  $\tau = 9.835$  ms, and  $\lambda = 0.089$  ms<sup>-1</sup>. Arrow indicates mean number of counts. Data adapted from Fig. 3 of the paper by Barlow and Levick (Ref. 5).

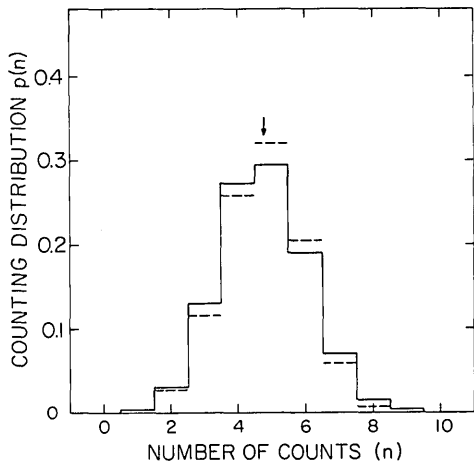


FIG. 17. Experimental PND (stepped histogram, 5000 samples) and theoretical fixed-dead-time PND (dashed lines) for an on-center unit at a background of 40 cd/m<sup>2</sup>. This corresponds to one data point in Fig. 15, for  $T = 100$  ms,  $\tau = 9.835$  ms, and  $\lambda = 0.089$  ms<sup>-1</sup>. Arrow indicates mean number of counts. Data adapted from Fig. 3 of the paper by Barlow and Levick (Ref. 5).

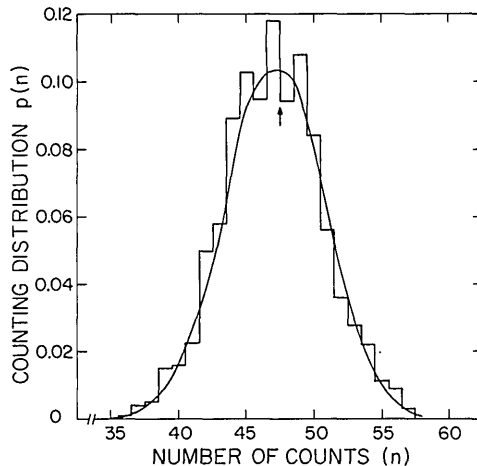


FIG. 19. Experimental PND (stepped histogram, 1000 samples) and theoretical fixed-dead-time PND (solid curve) for an on-center unit at a background of 40 cd/m<sup>2</sup>. This corresponds to one data point in Fig. 15, for  $T = 1.0$  s,  $\tau = 9.835$  ms, and  $\lambda = 0.089$  ms<sup>-1</sup>. Arrow indicates mean number of counts. Data adapted from Fig. 3 of the paper by Barlow and Levick (Ref. 5).

strong antibunching effects of the dead time can rapidly overpower intrinsic bunching effects which may be associated with a given distribution.<sup>23</sup> In Fig. 20, the solid curve represents the rate parameter  $\lambda$  (i.e., the average number of impulses per unit time that would be observed in the absence of dead time) as a function of luminance ( $L$ ), required to fit the data. Subtracting out the residual dark count ( $\bar{n} = 19$ ), we obtain the reduced rate parameter denoted by  $\lambda'$  (dotted curve) as the solution to  $\bar{n} - 19 = \lambda'T/(1 + \lambda'\tau)$ . The unique values for  $\tau$  used to calculate both  $\lambda$  and  $\lambda'$  are those shown in Table I and as the dashed curve in Fig. 20. The relationship between the luminance  $L$  and the rate parameters  $\lambda$  and  $\lambda'$ , namely a monotonically increasing curve in the plot of  $\lambda$  (or  $\lambda'$ ) versus  $\log L$ , appears similar to experimental data and to the relationship predicted by parametric feedback models.<sup>28,29</sup> In obtaining the reduced rate parameter  $\lambda'$ , we have assumed

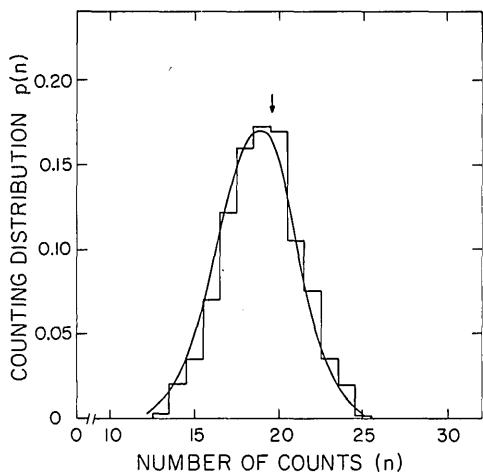


Fig. 18. Experimental PND (stepped histogram, 1000 samples) and theoretical fixed-dead-time PND (solid curve) for an on-center unit at a background of 40 cd/m<sup>2</sup>. This corresponds to one data point in Fig. 15, for  $T = 400$  ms,  $\tau = 9.835$  ms, and  $\lambda = 0.089$  ms<sup>-1</sup>. Arrow indicates mean number of counts. Data adapted from Fig. 3 of the paper by Barlow and Levick (Ref. 5).

(solely to enable us to perform the calculations easily) that the noise pulses are unaffected by any dead-time restrictions.

Equally interesting, perhaps, is the increase in average dead time with increasing luminance that is required to fit the observed statistics (fixed-dead-time approximation). One is led to conjecture, at least within the framework of the refractory model, that the inhibitory influence of the surround may be manifested in part as an increase in the average refractoriness of the ganglion cell. Observationally, of course, this relates to the increasing regularity of the discharge as the adaptation level is increased.

In Table II and in Fig. 21 we present the rate parameter  $\lambda$  (solid line) and dead time  $\tau$  (dashed line) required to fit the data for an off-center unit (JJ:3) adapted from Fig. 6 of the paper by Barlow and Levick.<sup>6</sup> Although the rate parameter  $\lambda$  varies only slightly with the luminance  $L$ , the dead time  $\tau$  again increases over the luminance range from  $3.4 \times 10^{-4}$  to 3.4 cd/m<sup>2</sup>. The behavior of  $\tau$  with  $L$  is very similar to that observed for the on-center unit (see Table I and Fig. 20) though for values of  $L < 3.4 \times 10^{-4}$  cd/m<sup>2</sup>,  $\tau$  appears to decrease with  $L$  for the off-center unit.

TABLE I. Fixed-dead-time model parameters for on-center unit DD:6 as a function of luminance. Data in columns 2 and 3 adapted from Fig. 6 of the paper by Barlow and Levick<sup>6</sup> (see Fig. 20).

$L$ (cd/m <sup>2</sup> )	$\bar{n}$	$\bar{n}/\sigma^2$	$\lambda$ (ms <sup>-1</sup> )	$\tau$ (ms)	$\lambda'$ (ms <sup>-1</sup> )
0	19	1.0	0.019	0.0	0.0
$3.4 \times 10^{-6}$	21	1.0	0.021	0.0	0.002
$3.4 \times 10^{-5}$	25	1.0	0.025	0.0	0.006
$3.4 \times 10^{-4}$	32	1.2	0.035	2.7	0.013
$3.4 \times 10^{-3}$	40	1.5	0.049	4.6	0.023
$3.4 \times 10^{-2}$	48	2.2	0.071	6.7	0.036
$3.4 \times 10^{-1}$	51	3.2	0.091	8.7	0.044
3.4	53	7.1	0.141	11.8	0.057

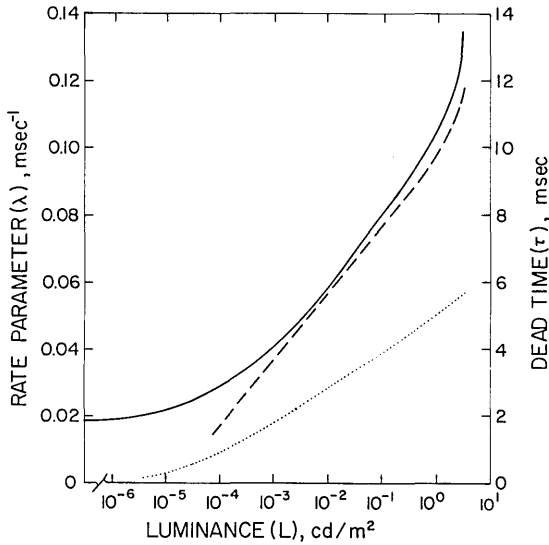


FIG. 20. Average dead time  $\tau$  (dashed curve) and rate parameter  $\lambda$  (solid curve) as a function of luminance for an on-center unit, as obtained from the fixed-dead-time model. The dotted line represents the reduced rate parameter  $\lambda'$  obtained by subtracting the zero-luminance (dark light) mean  $\bar{n} = 19$  from observed values of the mean.  $\lambda'$  is seen to be nearly proportional to  $\log L$  over some 4 orders of magnitude of variation in  $L$ . Raw data (see Table I) derived from Fig. 6 of the paper by Barlow and Levick (Ref. 6).

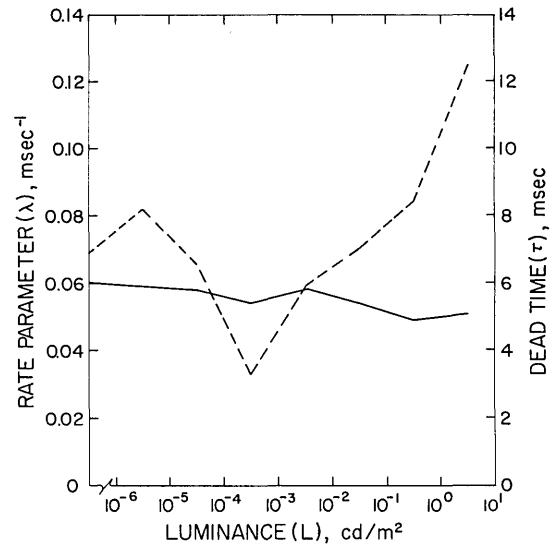


FIG. 21. Average dead time  $\tau$  (dashed curve) and rate parameter  $\lambda$  (solid curve) as a function of luminance for an off-center unit, as obtained from the fixed-dead-time model. Note that the rate parameter  $\lambda$  is virtually independent of  $L$  over more than 6 log units. The dependence of  $\tau$  on  $L$  is very similar to that obtained for the on-center unit (Fig. 20 and Table I) for  $L \geq 3.4 \times 10^{-4}$   $\text{cd}/\text{m}^2$ . Raw data (see Table II) derived from Fig. 6 of the paper by Barlow and Levick (Ref. 6).

## V. DISCUSSION

Using the general properties of the Poisson process, the effects of fixed and variable dead time on this process, and the relationship between pulse-number and pulse-interval distributions, we have been able to develop a consistent theoretical model that fits all of the data on the maintained discharge of the cat's retinal ganglion cell described by Barlow and Levick.<sup>5,6</sup> We have therefore brought together, within a single framework, the work of Rodieck,<sup>4,8</sup> Barlow and Levick,<sup>5,6</sup> and Barlow, Levick, and Yoon.<sup>13</sup> Specifically, the following three assumptions are implicit in our model: (i) Poisson process, (ii) nonparalyzable variable dead time that depends on luminance, and (iii) a small upward shift of the mean-to-variance ratio to separate away the effects of bunching at low luminance levels.

In this section we demonstrate the merit of this model in comparison with two alternative descriptions for the maintained discharge: scaling and paralyzable-dead-time counting. We also discuss the large values of dead time re-

TABLE II. Fixed-dead-time model parameters for off-center unit JJ:3 as a function of luminance. Data in columns 2 and 3 adapted from Fig. 6 of the paper by Barlow and Levick<sup>6</sup> (see Fig. 21).

$L$ ( $\text{cd}/\text{m}^2$ )	$\bar{n}$	$\bar{n}/\sigma^2$	$\lambda$ ( $\text{ms}^{-1}$ )	$\tau$ (ms)
0	43	2.0	0.060	6.9
$3.4 \times 10^{-6}$	40	2.2	0.059	8.2
$3.4 \times 10^{-5}$	42	1.9	0.058	6.6
$3.4 \times 10^{-4}$	46	1.4	0.054	3.3
$3.4 \times 10^{-3}$	43	1.8	0.058	5.9
$3.4 \times 10^{-2}$	39	1.9	0.054	7.0
$3.4 \times 10^{-1}$	35	2.0	0.049	8.5
3.4	31	2.7	0.051	12.6

quired by our model. We conclude the section with suggestions for future work.

### A. Scaling model

As discussed earlier (see Sec. I) the model considered by Barlow and Levick<sup>6</sup> assumed that  $r$  absorbed quanta were necessary to yield one ganglion cell spike (where  $r$  is the scaling parameter). For this case, the PID is the gamma distribution<sup>19</sup>

$$f(t) = \lambda(\lambda t)^{r-1} \exp(-\lambda t)/(r-1)!, \quad (21)$$

for  $r > 0$  and integer. Though Barlow and Levick<sup>5,6</sup> chose to fit their PND's by Gaussian distributions, this conjunction with the gamma PID does not form a consistent set within the framework of the scaling model. Since the gamma PID gives the waiting time to the  $r$ th pulse for a process obeying the Poisson probability law, the correct PND is<sup>19</sup>

$$p_r(n, T) = \sum_{k=rn}^{r(n+1)-1} [(\lambda T)^k/k!] \exp(-\lambda T), \quad (22)$$

where  $p_r(n, T)$  is the probability of registering  $n$  pulses in a time interval  $(0, T)$ . The mean  $\bar{n}_r$  and variance  $\sigma_r^2$  of this distribution are

$$\bar{n}_r = \lambda T/r \quad (23)$$

and

$$\sigma_r^2 = \lambda T/r^2, \quad (24)$$

respectively.

One of the major difficulties with this model is that the value of the scaling parameter calculated from Barlow and Levick's data<sup>6</sup> deviates by several orders of magnitude from the value needed to provide a good fit to the interval distributions; the fit is worse at high luminance levels. Furthermore, the gamma distribution does not provide a good fit to

the PID for off-center units. These authors<sup>6</sup> also obtain, at very low luminance levels, a value of  $r < 1$ , which was inexplicable in terms of the scaling model they presented. [More recently, Barlow, Levick, and Yoon<sup>13</sup> presented a multiple-path bunching model (see Sec. IV) to explain this behavior.] Barlow and Levick suggested two possible modifications to their scaling model to remedy the problems cited above. In the first, they presume that the scaling is imperfect, so that whereas the mean rate may be given by the rate of quantal absorptions divided by the scaling factor, the irregularity is caused, in large part, by added noise. In the second modification, the mean rate is assumed to be suppressed by the inhibitory influence of the surround which does not materially affect the noise. They suggest that results so far favor the second modification in which it is expected that the standard deviation of the quantal absorption rate divided by the scaling factor is equal to the standard deviation of the PND but that the mean rate would not be exactly predicted. (In the context of the present model we note that if the effect of the surround is associated with an increase in the effective dead time of the ganglion cell, both the mean firing rate and the variance of the PND would be suppressed.) Subsequently, Barlow<sup>12</sup> criticized the scaling model on other grounds as well. More recently, however, Stein<sup>15,16</sup> showed that a model incorporating both scaling and exponential decay (presumed to be associated with the membrane of the ganglion cell) also leads to a gamma distribution. Though the scaling parameter for this model corresponds with a larger range of luminance levels than the pure scaling model, the fit is still not satisfactory.<sup>9</sup>

### B. Paralyzable dead-time counter model

We also observe that a model based on the paralyzable (extended) dead-time counter<sup>18-21,55</sup> does not fit the ganglion cell data. In this case, even though events occurring during the dead-time period do not produce impulses, they nevertheless extend the period during which the counter does not respond. For a fixed dead time  $\tau$ , the asymptotic mean  $\bar{n}_\pi$ , the asymptotic variance  $\sigma_\pi^2$ , and the asymptotic mean-to-variance ratio  $\bar{n}_\pi/\sigma_\pi^2$  are given by<sup>19,55</sup>

$$\bar{n}_\pi \simeq \lambda T e^{-\lambda\tau}, \quad (25a)$$

$$\sigma_\pi^2 \simeq \lambda T e^{-\lambda\tau} - 2\lambda T(\lambda\tau)e^{-2\lambda\tau}, \quad (25b)$$

and

$$\bar{n}_\pi/\sigma_\pi^2 \simeq (1 - 2\lambda\tau e^{-\lambda\tau})^{-1}, \quad (25c)$$

respectively. Setting the derivative of Eq. (25c) equal to zero to determine the maxima and minima of the mean-to-variance ratio, we obtain

$$\frac{d(\bar{n}_\pi/\sigma_\pi^2)}{d(\lambda\tau)} = \frac{-2e^{-\lambda\tau}(\lambda\tau - 1)}{(1 - 2\lambda\tau e^{-\lambda\tau})^2} = 0. \quad (26)$$

The solution  $\lambda\tau = 1$  represents a maximum, indicating that  $\bar{n}_\pi/\sigma_\pi^2 \leq (1 - 2e^{-1})^{-1} \simeq 3.78$ . This is not consistent with the value 7.1 at 3.4 cd/m<sup>2</sup> in the data presented in Table I; we do not consider this model further here. The upper bound arises because the strongly driven paralyzable counter loses counts faster than the registrations become regularized. This is in distinction to the nonparalyzable counter which exhibits no upper bound for  $\bar{n}_\pi/\sigma_\pi^2$  [see Eq. (19)].

We note that the general type- $p$  counter, which reduces to paralyzable and nonparalyzable behavior as special cases, has

been considered by Albert and Nelson,<sup>56</sup> Bharucha-Reid,<sup>57</sup> and Parzen.<sup>19</sup> Use of this model would introduce another parameter, however.

### C. Long dead times

Although the values of dead time required for our model to fit the data are quite long (range 6.5–31 ms) in comparison with values normally considered as durations of an absolute refractory period (<2 ms), they are consistent with the values that Rodieck<sup>4</sup> has inferred via a different but related approach from his plots of standard deviation versus mean of the pulse-interval distributions, where he obtains an average dead time of 17.0 ms. It is worth noting that large values are not an artifact of the statistical approach since Goldberg, Adrian, and Smith,<sup>58</sup> using the same procedure employed by Rodieck, obtain a mean value of 1.9 ms for third-order superior olivary neurons in the auditory system. Although it is possible to interpret a sizeable portion of the dead time as arising from a relative refractory period (see below), it is possible that the dead time may be entirely due to a stochastic absolute refractory period. It is also worth noting the following: PID's for auditory nerve fibers contain many very large intervals between successive impulses at all stimulus levels. Thus, for example, an auditory neuron may not respond to 20 or more successive 1000 Hz sinusoidal fluctuations at 90 dB above the neuron's threshold (corresponding to a delay time of 20 ms) but may respond to two successive fluctuations at 30 dB above threshold.<sup>59</sup> Such lack of sensitivity to intensity change could reflect a stochastic dead time following an impulse. As noted above, dead times for superior olivary neurons appear to conform to more normally expected values of refractory periods. Thus it is possible that neurons receiving inputs from presynaptic units with graded potentials may have very long refractory periods for stimulation via normal synaptic routes (not via extrinsically applied electrical stimulation of the neuron) relative to those normally observed in units receiving inputs from presynaptic units generating spikes.

### D. Extensions

Although the model we have presented considers only the one-dimensional PID's and PND's, it can be extended to deal with successive intervals that are not independent. Such an extension would be able to readily incorporate the serial correlation coefficients of the interval distribution (Kuffler, FitzHugh, and Barlow<sup>1</sup> have observed correlations between adjacent interspike intervals to range between 0 and -0.25, and Rodieck<sup>4</sup> has reported values between -0.21 and +0.11 with an average of -0.06). A likely way to do this is to assign a large part of the dead time in the model to a relative refractory period during which the neuron recovers sensitivity gradually, and a smaller portion to an absolute refractory period. (The values of  $\bar{\tau}$  and  $\sigma_\tau^2$  we have obtained here are compatible with such a division.) If the recovery process following a sequence of two impulses is slower when the interval between the two is shorter, a negative serial correlation would result. It may be, however, that the observed dependencies are in the transfer of information between the absorption of quanta by photoreceptors and the ganglion cell wherein, for example, excitation via one path is accompanied by an inhibition of conduction via adjacent paths either simultaneously or shortly afterward. In this connection it is worth noting that Rodieck<sup>4</sup> observes frequent significant cross

correlations between the discharges from two nearby neurons following the occurrence of a spike in one of them. Rodieck has also observed that both the joint-interval histogram and the serial correlation coefficients can be used to demonstrate the statistical dependence between time intervals, which varies from unit to unit, and is not revealed by the autocorrelogram. Forward and backward recurrence-time experiments<sup>60</sup> could also be performed on adjacent ganglion cells to better quantify the statistical dependence over short time intervals (less than 1 s).

Retinal ganglion cells do not appear to be a single group, but have been classified into *X* and *Y* cells<sup>61,62</sup> and *W* cells,<sup>63</sup> although it has also been suggested that *X* and *Y* cells may be ends of a continuous distribution of units.<sup>64</sup> The units for which Barlow and Levick<sup>6</sup> presented PID's and PND's were not chosen with respect to these classifications, and it will be desirable to determine how the present model fits different varieties.<sup>65</sup> Finally we note that our model, although providing good fits to the maintained discharge, has not yet been applied to transient responses.<sup>66</sup> Indeed it may also apply to preparations simpler than the cat's ganglion cell, e.g., *Limulus*.<sup>55,67,68</sup>

## ACKNOWLEDGMENT

The authors are grateful to R. W. Rodieck, L. M. Ricciardi, P. Diamant, and B. Wandell for critically reading the manuscript and for providing many helpful suggestions.

## APPENDIX A: CALCULATION OF THE EXACT VARIABLE-DEAD-TIME PID

Let us represent by  $F(t)$  the probability that the time of occurrence of a second pulse, after the registration of a first pulse, is less than  $t$  seconds. As previously,  $1 - F(t)$  represents the probability that zero pulses occur in the time interval  $t$ . There are now two independent ways in which this can occur: (i)  $t < \tau$ , and (ii)  $t > \tau$ , and 0 pulses occur in the interval  $(\tau, t)$ . Thus for the memoryless Poisson process<sup>48</sup>

$$1 - F(t) = \int_0^\infty P(\tau) d\tau + \int_0^t P(\tau)p(0, t - \tau) d\tau, \quad (A1)$$

where  $p(0, t - \tau)$  represents the probability that exactly zero pulses occur in the interval  $(\tau, t)$ . Differentiation of Eq. (A1) with respect to  $t$  yields the desired pulse-interval distribution,

$$f(t) = P(t) - (\partial/\partial t) \left[ \int_0^t P(\tau)p(0, t - \tau) d\tau \right]. \quad (A2)$$

This is the simplest general expression which can be obtained for  $f(t)$  inasmuch as the integral in Eq. (A2) must be evaluated for the particular distribution  $P(\tau)$  under consideration.

We recall that for a Poisson process,  $p(n, T)$  is given by Eq. (5); for  $P(\tau)$  we choose the relatively simple distribution

$$P(\tau) = c^{-1}(2\pi)^{-1/2}\sigma_\tau^{-1} \exp[-(2\sigma_\tau^2)^{-1}(\tau - \bar{\tau})^2], \quad \tau \geq 0 \quad (A3)$$

which is a truncated Gaussian, since  $\tau < 0$  is forbidden. The quantity  $c$  is the normalization constant and is given by

$$c = 1/2 \operatorname{erfc}[-\bar{\tau}/(2^{1/2}\sigma_\tau)]. \quad (A4)$$

The function  $\operatorname{erfc}x$  is the complementary error function evaluated at  $x$ , which is defined by the integral

$$\operatorname{erfc}x = 2\pi^{-1/2} \int_x^\infty e^{-u^2} du, \quad (A5)$$

and has been tabulated.<sup>53</sup> The integral in Eq. (A2) thus becomes

$$\int_0^t P(\tau)p(0, t - \tau) d\tau = c^{-1}(2\pi)^{-1/2}\sigma_\tau^{-1} \times \int_0^t \exp[-(2\sigma_\tau^2)^{-1}(\tau - \bar{\tau})^2] \exp[-\lambda(t - \tau)] d\tau. \quad (A6)$$

Combining the exponents and completing the square, this is evaluated as

$$\int_0^t P(\tau)p(0, t - \tau) d\tau = c^{-1} \exp - [\lambda(t - \bar{\tau}) - 1/2(\sigma_\tau\lambda)^2] \times \{ \operatorname{erfc}[-(t - \bar{\tau} - \sigma_\tau^2\lambda)/(2^{1/2}\sigma_\tau)^{-1}] - \operatorname{erfc}[(\bar{\tau} + \sigma_\tau^2\lambda)/(2^{1/2}\sigma_\tau)^{-1}] \}. \quad (A7)$$

Using Eqs. (A2), (A4), and (A7), the exact pulse-interval distribution for a Poisson process with a Gaussian-distributed dead time is found to be

$$f(t) = \frac{\lambda}{2} \left[ \exp - \left( \lambda(t - \bar{\tau}) - \frac{(\sigma_\tau\lambda)^2}{2} \right) \right] \left[ \frac{1}{2} \operatorname{erfc} \left( \frac{-\bar{\tau}}{2^{1/2}\sigma_\tau} \right) \right]^{-1} \times \left[ \operatorname{erfc} \left( -\frac{t - \bar{\tau} - \sigma_\tau^2\lambda}{2^{1/2}\sigma_\tau} \right) - \operatorname{erfc} \left( \frac{\bar{\tau} + \sigma_\tau^2\lambda}{2^{1/2}\sigma_\tau} \right) \right]. \quad (A8)$$

An alternate method of obtaining the pulse-interval distribution given in Eq. (A8) is to average the distribution for a fixed dead time, given in Eq. (9), over the variation in the dead time, given by  $P(\tau)$ .<sup>24</sup> This provides a convenient check on the result presented in Eq. (A8), as both methods yield the same result. Rodieck's<sup>4,8</sup> computer simulation relates to this latter method.

## APPENDIX B: CALCULATION OF THE APPROXIMATE VARIABLE-DEAD-TIME PND

The PND for the variable-dead-time case is obtained with the help of Eq. (15) as

$$p(n, T, \bar{\tau}, \sigma_\tau) = \langle p(n, T | \tau_1, \tau_2, \dots, \tau_n) \rangle_{\{\tau_i\}}, \quad \{\tau_i\} = \{\tau_1, \tau_2, \dots, \tau_n\}, \quad (B1)$$

where the angular brackets represent an ensemble average over the statistics of  $\{\tau_i\}$ ; the argument of the total probability now reflects its dependence on the mean and variance of the dead time,  $\bar{\tau}$  and  $\sigma_\tau^2$ , respectively.

If each of the dead times  $\tau_i$  is assumed to be an independent sample of the underlying random variation of the dead time, the  $\tau_i$ 's can be treated as identically distributed independent random variables. Furthermore, the distribution of each  $\tau_i$  is now chosen to be precisely Gaussian with mean  $\bar{\tau}$  and variance  $\sigma_\tau^2$  so that the distribution of the sum  $\tau_1 + \tau_2 + \dots + \tau_n$  will be Gaussian with mean  $n\bar{\tau}$  and variance  $n\sigma_\tau^2$ . The choice of a Gaussian distribution for the dead time is an approximation, since in reality, the dead time  $\tau$  cannot be less than 0, which is why we truncated the distribution in Eq. (A3). The Gaussian approximation will be reasonably good when

the mean dead time  $\bar{\tau}$  is larger than the standard deviation  $\sigma_\tau$ . This insures that the portion of the dead-time distribution below  $\tau = 0$  is small. This is the case throughout this paper.

Formally, we define  $T_n$  as

$$T_n = \tau_1 + \tau_2 + \dots + \tau_n. \quad (B2)$$

Since the  $\tau_i$ 's appear only as a sum in Eq. (15), we can write the conditional counting distribution as

$$\begin{aligned} p(n, T | \tau_1, \tau_2, \dots, \tau_n) &= p(n, T | T_n) \\ &= \sum_{k=0}^n \{\lambda^k [T - T_n]^k / k!\} \exp\{-\lambda[T - T_n]\} \\ &\quad - \sum_{k=0}^{n-1} \{\lambda^k [T - T_{n-1}]^k / k!\} \exp\{-\lambda[T - T_{n-1}]\}, \end{aligned} \quad n \geq 1 \quad (B3)$$

for  $T > T_n$ , so that the total probability is

$$p(n, T, \bar{\tau}, \sigma_\tau) = \int_{-\infty}^{\infty} p(n, T | T_n) P(T_n | n, T) dT_n. \quad (B4)$$

The quantity  $P(T_n | n, T)$  is the conditional probability of  $T_n$  given  $n$  and  $T$ . This is in general difficult to evaluate. For counting intervals  $T \gtrsim n\bar{\tau} + 2n^{1/2}\sigma_\tau$ , however,  $P(T_n | n, T)$  can be approximated by the unconditional distribution of the sum of the  $\tau_i$ 's, given by

$$P(T_n) = (2\pi)^{-1/2} \sigma_{T_n}^{-1} \exp\{-(2\sigma_{T_n}^2)^{-1}(T_n - \bar{T}_n)^2\}, \quad (B5)$$

with

$$\bar{T}_n = n\bar{\tau} \quad (B6)$$

and

$$\sigma_{T_n}^2 = n\sigma_\tau^2. \quad (B7)$$

This is simply a Gaussian distribution. Combining Eqs. (B3) and (B4), the total probability becomes

$$\begin{aligned} p(n, T, \bar{\tau}, \sigma_\tau) &\simeq \int_{-\infty}^T \left( \sum_{k=0}^n \{\lambda^k [T - T_n]^k / k!\} \exp\{-\lambda[T - T_n]\} \right. \\ &\quad \left. - \sum_{k=0}^{n-1} \{\lambda^k [T - T_{n-1}]^k / k!\} \exp\{-\lambda[T - T_{n-1}]\} \right) P(T_n) dT_n; \end{aligned} \quad (B8)$$

the upper limit on the integral reflects the fact that  $p(n, T | T_n) = 0$  for  $T_n > T$ . Since the sums within the integral are finite, the order of summation and integration can be interchanged, leading us to seek integrals of the form

$$p_{k,n} \simeq \int_{-\infty}^T \{\lambda^k [T - T_n]^k / k!\} \exp\{-\lambda[T - T_n]\} P(T_n) dT_n, \quad (B9)$$

with  $P(T_n)$  given in Eqs. (B5), (B6), and (B7).

The integral can be evaluated in terms of the  $n$ th-iterated integrals of the complementary error function, denoted  $i^n \text{erfcx}$ . These are tabulated functions<sup>53</sup> and are defined as

$$\begin{aligned} i^n \text{erfcx} &= \int_x^\infty i^{n-1} \text{erfcu} du, \\ i^0 \text{erfcx} &= \text{erfcx}, \quad i^{-1} \text{erfcx} = 2\pi^{-1/2} \exp(-x^2). \end{aligned} \quad (B10)$$

It is also possible to express  $i^n \text{erfcx}$  in terms of a single integral as

$$i^n \text{erfcx} = (2\pi^{-1/2}/n!) \int_x^\infty (u-x)^n \exp(-u^2) du; \quad (B11)$$

the function satisfies the recurrence relation

$$2ni^n \text{erfcx} + 2xi^{n-1} \text{erfcx} = i^{n-2} \text{erfcx}. \quad (B12)$$

After some algebra, it can be shown that the  $p_{k,n}$  are

$$\begin{aligned} p_{k,n} &\simeq \frac{1}{2} [\lambda 2^{1/2} n^{1/2} \sigma_\tau]^k \exp\{-\lambda[T - n\bar{\tau}] - \frac{1}{2} n \sigma_\tau^2 \lambda^2\} \\ &\quad \times i^k \text{erfc}\{-(T - n\bar{\tau} - n\lambda \sigma_\tau^2) / (2^{1/2} n^{1/2} \sigma_\tau)^{-1}\}, \end{aligned} \quad (B13)$$

and the total probability is therefore given by

$$p(n, T, \bar{\tau}, \sigma_\tau) \simeq \sum_{k=0}^n p_{k,n} - \sum_{k=0}^{n-1} p_{k,n-1}, \quad n \geq 1. \quad (B14)$$

Of course, the total dead time  $T_n$  must be  $\geq 0$ . As an indication of the validity of the Gaussian approximation, the integral represented in Eq. (B9), but now with limits from  $-\infty$  to 0, is found to be

$$\begin{aligned} &\sum_{m=0}^k [(k-m)!]^{-1} [T / (2^{1/2} n^{1/2} \sigma_\tau)]^{k-m} \\ &\quad \times i^m \text{erfc}\{(n\bar{\tau} + n\sigma_\tau^2 \lambda) / (2^{1/2} n^{1/2} \sigma_\tau)\}. \end{aligned} \quad (B15)$$

For the data that we consider, these terms contribute only about  $10^{-8}$  to the probability, whereas the  $p_{k,n}$  in Eq. (B13) contribute  $\sim 10^{-1}$ .

\*This work was supported by the Public Health Service through the National Institutes of Health under Grant No. 1R03 MH 23425 from the National Institute of Mental Health and under Grant No. 2R01 EY 00375 from the National Eye Institute, and by the National Science Foundation under Grant Nos. ENG75-09325 and BMS73-01463 A01.

<sup>1</sup>S. W. Kuffler, R. FitzHugh, and H. B. Barlow, "Maintained activity in the cat's retina in light and darkness," *J. Gen. Physiol.* **40**, 683-702 (1957).

<sup>2</sup>T. Ogawa, P. O. Bishop, and W. R. Levick, "Temporal characteristics of responses to photic stimulation by single ganglion cells in the unopened eye of the cat," *J. Neurophysiol.* **29**, 1-30 (1966).

<sup>3</sup>M. Straschill, "Aktivität von Neuronen im Tractus opticus und Corpus geniculatum laterale bei langdauernden Lichtreizen verschiedener Intensität," *Kybernetik* **3**, 1-8 (1966).

<sup>4</sup>R. W. Rodieck, "Maintained activity of cat retinal ganglion cells," *J. Neurophysiol.* **30**, 1043-1071 (1967).

<sup>5</sup>H. B. Barlow and W. R. Levick, "Three factors limiting the reliable detection of light by the retinal ganglion cells of the cat," *J. Physiol. (London)* **200**, 1-24 (1969).

<sup>6</sup>H. B. Barlow and W. R. Levick, "Changes in the maintained discharge with adaptation level in the cat retina," *J. Physiol. (London)* **202**, 699-718 (1969).

<sup>7</sup>B. Sakmann and O. D. Creutzfeldt, "Scotopic and mesopic light adaptation in the cat retina," *Pfluegers Arch. Gesamte Physiol. Menschen Tiere* **313**, 168-185 (1969).

<sup>8</sup>R. W. Rodieck, *The Vertebrate Retina* (Freeman, San Francisco, 1973), pp. 646-672.

<sup>9</sup>W. R. Levick, "Maintained discharge in the visual system and its role for information processing," in *Handbook of Sensory Physiology*, Vol. VII/3, *Central Processing of Visual Information*, Part A, edited by R. Jung (Springer-Verlag, New York, 1973), pp. 575-598.

<sup>10</sup>R. T. Marrocco, "Maintained activity of monkey optic tract fibers and lateral geniculate nucleus cells," *Vision Res.* **12**, 1175-1181 (1972).

<sup>11</sup>E. A. Trabka, "Effect of scaling optic-nerve impulses on incremental thresholds," *J. Opt. Soc. Am.* **59**, 345-349 (1969).

<sup>12</sup>H. B. Barlow, "Scaling and refractoriness in pulse trains," *J. Opt. Soc. Am.* **59**, 1500 (1969).

<sup>13</sup>H. B. Barlow, W. R. Levick, and M. Yoon, "Responses to single

- quanta of light in retinal ganglion cells of the cat," *Vision Res.* 11 (Suppl. 3), 87–101 (1971).
- <sup>14</sup>"Bibliography on Dead Time Effects," Bureau International des Poids et Mesures, Sèvres, France, Report No. BIPM-75/6, 1975, edited by J. W. Müller (unpublished).
- <sup>15</sup>R. B. Stein, "A theoretical analysis of neuronal variability," *Biophys. J.* 5, 173–194 (1965).
- <sup>16</sup>R. B. Stein, "Some models of neuronal variability," *Biophys. J.* 7, 37–68 (1967).
- <sup>17</sup>C. J. Gundersdorf, "A new method for determining some statistical properties of light," in *Quantum Limitations on Optical Communications*, Johns Hopkins Carlyle Barton Laboratory, Tech. Report No. AFAL-TR-71-58, DDC No. AD882879, April 1971, pp. 76–175 (unpublished).
- <sup>18</sup>W. Feller, "On probability problems in the theory of counters," in *Studies and Essays: A Volume for the Anniversary of Courant* (Wiley, New York, 1948), pp. 105–115.
- <sup>19</sup>E. Parzen, *Stochastic Processes* (Holden-Day, San Francisco, 1962), pp. 117–186.
- <sup>20</sup>I. DeLotto, P. F. Manfredi, and P. Principi, "Counting statistics and dead-time losses, Part 1," *Energ. Nucl. (Milan)* 11, 557–564 (1964).
- <sup>21</sup>J. W. Müller, "Dead-time problems," *Nucl. Instrum. Methods* 112, 47–57 (1973).
- <sup>22</sup>J. W. Müller, "Some formulae for a dead-time-distorted Poisson process," *Nucl. Instrum. Methods* 117, 401–404 (1974).
- <sup>23</sup>B. I. Cantor and M. C. Teich, "Dead-time-corrected photocounting distributions for laser radiation," *J. Opt. Soc. Am.* 65, 786–791 (1975).
- <sup>24</sup>P. A. Lee, "Output response of non-linear switching element with stochastic dead time," *Kybernetik* 15, 187–191 (1974).
- <sup>25</sup>L. M. Ricciardi and F. Esposito, "On some distribution functions for non-linear switching elements with finite dead time," *Kybernetik* 3, 148–152 (1966).
- <sup>26</sup>G. Bédard, "Dead-time corrections to the statistical distribution of photoelectrons," *Proc. Phys. Soc. (London)* 90, 131–141 (1967).
- <sup>27</sup>G. W. Hughes and L. Maffei, "On the origin of the dark discharge of retinal ganglion cells," *Arch. Ital. Biol.* 103, 45–59 (1965).
- <sup>28</sup>M. G. F. Fuortes and A. L. Hodgkin, "Changes in time scale and sensitivity in the ommatidia of limulus," *J. Physiol. (London)* 172, 239–263 (1964).
- <sup>29</sup>L. Marin, "Critical duration, the differential luminance threshold, critical flicker frequency, and visual adaptation: A theoretical treatment," *J. Opt. Soc. Am.* 58, 404–415 (1968).
- <sup>30</sup>G. Sperling and M. M. Sondhi, "Model for visual luminance discrimination and flicker detection," *J. Opt. Soc. Am.* 58, 1133–1145 (1968).
- <sup>31</sup>J. Levinson, "One stage model for visual temporal integration," *J. Opt. Soc. Am.* 56, 95–97 (1966).
- <sup>32</sup>J. A. J. Roufs, "Dynamic properties of vision—II. Theoretical relationships between flicker and flash thresholds," *Vision Res.* 12, 279–292 (1972).
- <sup>33</sup>D. H. Kelly, "Flicker," in *Handbook of Sensory Physiology*, Vol. VII/4, *Visual Psychophysics*, edited by D. Jameson and L. M. Hurvich (Springer-Verlag, New York, 1972), pp. 273–302.
- <sup>34</sup>W. A. van de Grind, O. J. Grüsser, and H. W. Lunkenheimer, "Temporal transfer properties of the afferent visual system, psychophysical, neurophysiological and theoretical investigations," in *Handbook of Sensory Physiology*, Vol. VII/3, *Central Processing of Visual Information*, Part A, edited by R. Jung (Springer-Verlag, New York, 1973), pp. 431–573.
- <sup>35</sup>R. D. DeVoe, "A nonlinear model for transient responses from light-adapted wolf spider eyes," *J. Gen. Physiol.* 50, 1993–2030 (1967).
- <sup>36</sup>M. Aguilar and W. S. Stiles, "Saturation of the rod mechanism at high levels of stimulation," *Opt. Acta* 1, 59–65 (1954).
- <sup>37</sup>M. C. Teich and W. J. McGill, "Neural counting and photon counting in the presence of dead time," *Phys. Rev. Lett.* 36, 754–758; 1473 (1976).
- <sup>38</sup>A. V. Holden, "Models of the stochastic activity of neurones," in *Lecture Notes in Biomathematics*, edited by S. Levin (Springer-Verlag, New York, 1976), Vol. 12.
- <sup>39</sup>C. Palm, "Intensitätsschwankungen im Fernsprechverkehr," *Ericsson Tech. (Stockholm)* 44, 1–189 (1943).
- <sup>40</sup>D. R. Cox and W. L. Smith, "The superposition of several strictly periodic sequences of events," *Biometrika* 40, 1–11 (1953).
- <sup>41</sup>D. R. Cox and W. L. Smith, "On the superposition of renewal processes," *Biometrika* 41, 91–99 (1954).
- <sup>42</sup>E. Çinlar, "Superposition of point processes" in *Stochastic Point Processes: Statistical Analysis, Theory, and Applications*, edited by P. A. W. Lewis (Wiley, New York, 1972), pp. 549–606.
- <sup>43</sup>W. J. McGill, "Neural counting mechanisms and energy detection in audition," *J. Math. Psychol.* 4, 351–376 (1967).
- <sup>44</sup>R. J. Glauber, "Photon fields and classical fields," in *Symposium on Modern Optics*, edited by J. Fox (Polytechnic, Brooklyn, New York, 1967), pp. 1–18.
- <sup>45</sup>B. Souček, "Losses in systems with variable dead time," *Nucl. Instrum. Methods* 27, 306–308 (1964).
- <sup>46</sup>I. DeLotto and P. F. Manfredi, "Time-distribution of events at the output of systems with variable dead-time," *Energ. Nucl. (Milan)* 12, 95–97 (1965).
- <sup>47</sup>I. DeLotto and P. F. Manfredi, "Statistical behavior of systems with variable dead-time," *Nucl. Instrum. Methods* 32, 175–176; 34, 180 (1965).
- <sup>48</sup>L. Kleinrock, *Queueing Systems Volume 1: Theory* (Wiley, New York, 1975).
- <sup>49</sup>C. Bendjaballah and F. Perrot, "Statistical properties of intensity-modulated coherent radiation. Theoretical and experimental aspects," *J. Appl. Phys.* 44, 5130–5141 (1973).
- <sup>50</sup>G. Lachs and D. R. Voltmer, "Photocount time interval distribution for superposed coherent and chaotic radiation," *J. Appl. Phys.* 47, 346–349 (1976).
- <sup>51</sup>W. L. Smith, "On renewal theory, counter problems, and quasi-Poisson processes," *Camb. Phil. Soc.* 53, 175–193 (1957).
- <sup>52</sup>W. L. Smith, "Renewal theory and its ramifications," *J. R. Stat. Soc., Sec. B* 20, 243–302 (1958).
- <sup>53</sup>*Handbook of Mathematical Functions with Formulas, Graphs, and Mathematical Tables*, edited by M. Abramowitz and I. A. Stegun, Nat. Bur. Stds. (U.S.) Appl. Math. Ser., U.S. Govt. Printing Office, Washington, D.C., 1964 (Dover, New York, 1965).
- <sup>54</sup>B. I. Cantor, L. Marin, and M. C. Teich, "Photocounting distributions with variable dead time," *Appl. Opt.* 14, 2819–2820 (1975).
- <sup>55</sup>C. G. Mueller, "A quantitative theory of visual excitation for the single photoreceptor," *Proc. Nat. Acad. Sci. USA* 40, 853–863 (1954).
- <sup>56</sup>G. E. Albert and L. Nelson, "Contributions to the statistical theory of counter data," *Ann. Math. Stat.* 24, 9–22 (1953).
- <sup>57</sup>A. T. Bharucha-Reid, *Elements of the Theory of Markov Processes and their Applications* (McGraw-Hill, New York, 1960), Chap. 6.3.
- <sup>58</sup>J. M. Goldberg, H. O. Adrian, and F. D. Smith, "Response of neurons of the superior olivary complex of the cat to acoustic stimuli of long duration," *J. Neurophysiol.* 27, 706–749 (1964).
- <sup>59</sup>J. E. Rose, J. F. Brugge, D. J. Anderson, and J. E. Hind, "Phase-locked response to low-frequency tones in single auditory nerve fibers of the squirrel monkey," *J. Neurophysiol.* 30, 769–793 (1967).
- <sup>60</sup>D. H. Johnson and N. Y. S. Kiang, "Analysis of discharges recorded simultaneously from pairs of auditory nerve fibers," *Biophys. J.* 16, 719–734 (1976).
- <sup>61</sup>C. Enroth-Cugell and J. G. Robson, "The contrast sensitivity of retinal ganglion cells of the cat," *J. Physiol. (London)* 187, 517–552 (1966).
- <sup>62</sup>H. Ikeda and M. J. Wright, "Receptive field organisation of 'sustained' and 'transient' retinal ganglion cells which subserved different functional roles," *J. Physiol. (London)* 222, 769–800 (1972).
- <sup>63</sup>J. Stone and Y. Fukuda, "Properties of cat retinal ganglion cells: a comparison of W-cells with X- and Y-cells," *J. Neurophysiol.* 37, 722–748 (1974).
- <sup>64</sup>J. L. Zacks, "Changes in responses of X and Y type cat retinal ganglion cells produced by changes in background illumination," presented at the Annual Meeting of the Association for Research in Vision and Ophthalmology (ARVO), Sarasota, April 1975 (unpublished).
- <sup>65</sup>T. Sato, M. Yamamoto, and H. Nakahama, "Variability of interspike intervals of cat's on-center optic tract fibres activated by steady light spot: A comparative study on X- and Y-fibres," *Exp. Brain Res.* 24, 285–293 (1976).

<sup>66</sup>R. W. Winters and J. W. Walters, "Transient and steady state stimulus-response relations for cat retinal ganglion cells," *Vision Res.* 10, 461-477 (1970).  
<sup>67</sup>L. A. Riggs, "Recovery from the discharge of an impulse in a single

visual receptor unit," *J. Cell. Comp. Physiol.* 15, 273-283 (1940).

<sup>68</sup>H. K. Hartline and F. Ratliff, *Studies on Excitation and Inhibition in the Retina* (Rockefeller Press, New York, 1974).

# Subjective Lorentz transformations and the perception of motion\*

Terry Caelli, William Hoffman,<sup>†</sup> and Harold Lindman<sup>‡</sup>

*Psychology Department, University of Melbourne, Parkville, Victoria, Australia 3052*

(Received 9 August 1977; revision received 2 November 1977)

It has been known for some 40 years that the perceived velocity of a moving object does not correspond to its physical velocity. It is also known that the perceived length and temporal duration of a moving object is affected by its physical velocity. In this paper it is argued that such phenomenal distortions can be embedded in a model for motion perception that involves the concepts of moving frames, Lorentz transformations, perceived length contractions, and time dilations. Experimental results support this model and indicate that  $c^*$ , the maximum perceivable velocity of movement, plays a crucial role in determining motion effects.

## I. INTRODUCTION

The problem of how we perceive movement has been a perennial object of investigation.<sup>1,2</sup> Such factors as distance, size, homogeneity and structure of background, orientation of the direction of movement, brightness, and mode of observation affect the perception of velocity.<sup>3</sup> Similarly, the velocity of a moving stimulus is known to have specific effects on the static parameters of the perceived shape. For example, it is known that the apparent length of a moving object decreases as its velocity increases both in linear<sup>4</sup> and rotary directions of motion.<sup>5</sup>

One puzzling observation which has intrigued many investigators is that perceived velocity is not proportional to physical velocity in terms of the (Galilean) distance-to-time ratio.<sup>6</sup> These results indicate that subjective estimates of visual spatio-temporal events undergoing motion are inconsistent with a Galilean perspective of the visual space-time geometry: a perspective that does not consider the relative nature of such estimates.<sup>7,8</sup>

We propose here a model for motion perception which incorporates the relativity of subjective space-time estimates and we argue that many of the questions posed by previous data can be answered by the proposition that a visual form of the Lorentz transformations governs the visual processing of movement. An important result of this formation will be that the geometrical structure of perceived space-time constitutes a Riemannian space of negative curvature (hyperbolic geometry), governed largely by the maximum velocity of perceived movement.

## II. THE REFERENCE FRAMES FOR PERCEIVED MOTION

In order to distinguish between, what we term, the physical and perceptual frames of reference, consider a light source translating horizontally at velocity  $v$  with respect to a stationary observer. Here there are two physical frames: one

moving [P1, Fig. 1(a)] at velocity  $v$  with respect to the stationary (observer) frame [P2, Fig. 1(a)]. In this system signals propagate at the speed of light,  $c$ , and no distortions would occur in the detection of velocities within the range of human velocity perception (40-100 deg/s, Refs. 1 and 9). This system assumes that the detector can process velocities at the speed of light.

However, the perceptual frames of reference are more limited. If we regard P2, the physical stationary frame, as having a human observer centered at its origin [S2, Fig. 1(b)], then the observer's processing of the velocity of the moving object [S1, Fig. 1(b)] is limited by the maximum velocity of perceived movement,  $c^*$ . This maximum velocity is considerably lower than the physical propagation rate of light ( $c^* \ll c$ ) and is a measure of the finite propagation rate of signals in the human visual system.<sup>10</sup> Such limitations are possibly due to a variety of phenomena from retinal persistence to more general finite neural propagation rates along the visual pathways.

Past treatments of the problem of movement perception have invariably assumed that the subjective frames S1 and

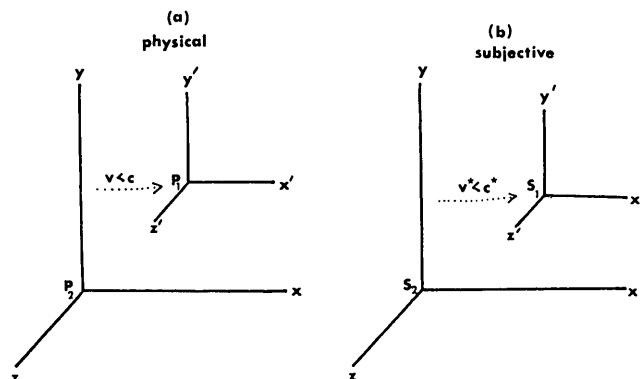


FIG. 1. Physical (a) and subjective (b) frames of reference: standard configurations.